Received: 22 October 2022 | Revised: 18 April 2023 | Accepted: 11 September 2023

DOI: 10.1002/acs.3684

RESEARCH ARTICLE

WILEY

Hybrid two-stage adaptive maximum power point tracking for stand-alone, grid integration, and partial shaded PV system

Saibal Manna[1,2] | **Deepak Kumar Singh**[1] | **Ashok Kumar Akella**[1]

[1]Department of Electrical Engineering, National Institute of Technology Jamshedpur, Jamshedpur, India

[2]Department of Electrical and Electronics Engineering, ABES Engineering College, Ghaziabad, India

Correspondence
Saibal Manna, Department of Electrical Engineering, National Institute of Technology Jamshedpur, Jamshedpur, Jharkhand-831014, India.
Email: mannasaibal1994@gmail.com

Summary

In a PV array, the power-voltage characteristic (P-V) and output power are completely dependent on atmospheric conditions. Consequently, the P-V curve's maximum power point (MPP) likewise changes significantly. This abrupt oscillation in the MPP may be caused by the PV panel being uniformly or partially shaded by trees, buildings, raindrops, and clouds. However, in both circumstances, the maximum power point tracking (MPPT) turns into a highly nonlinear issue with a time-bounded solution. The unpredictable weather circumstances change P-V characteristics after every short time interval. Therefore, this research presents a hybrid two-stage adaptive MPPT to overcome the environmental uncertainties. The first stage is MPPT control block for determining reference voltage for each MPP and the second stage is modified model reference adaptive controller (MMRAC) block fine-tunes converter duty cycle to maintain MPP of PV panel. The probabilistic evaluation is executed through four distinct levels of uncertainty, including stand-alone, partially-shaded, grid integration, and OPAL-RT to examine the system robustness in diverse scenario. The possibility of the tracking failure caused by dynamic irradiance change is also verified. Moreover, efficiency, tracking ability, power loss, ripple, and error rate are compared with the state-of-the-art strategies, that is, ANFIS, INC, P&O, and VSPO. The satisfactory performances of the new strategy under simultaneously varying irradiance, temperature, and load; partially shaded and grid integration shows the supremacy.

KEYWORDS

grid-integration, maximum power point tracking, modified MRAC, MPPT failure, partial shading, solar PV

1 | INTRODUCTION

1.1 | Motivation

Many countries throughout the globe, led by the United States and China, have recently pledged to reduce greenhouse gas emissions in order to develop a future energy system with low carbon intensity. Distributed energy resources (DERs)

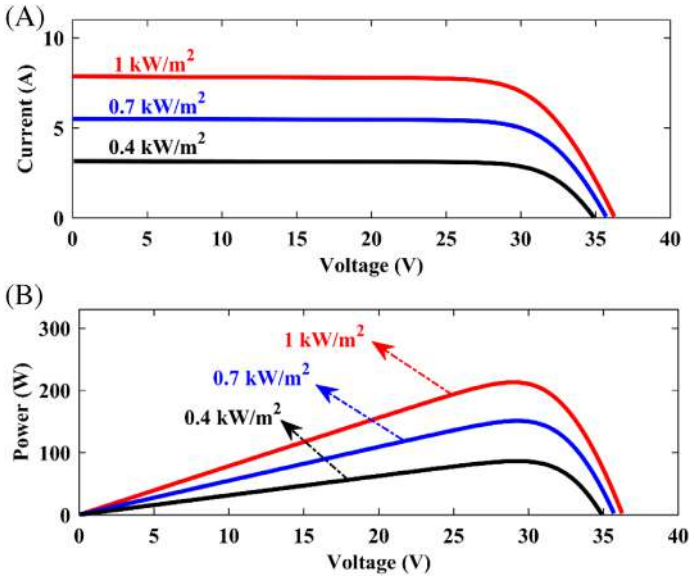

FIGURE 1 Characteristics of (A) I-V and (B) P-V at varying irradiance (kW/m^2).

based on renewable sources are essential to achieving a carbon-free energy sector transformation.[1] Among the DERs that already exist, solar photovoltaics (SPV) are the most widespread, cost-effective, and potential renewable energy source that can provide a lot of energy for users.[2] Also, pollution-free operation, scalability, a lack of fuel costs, and cheap maintenance requirements are all advantages of PV generating systems. There are, however, a number of drawbacks to using photovoltaic (PV) energy generation, including low efficiency, the expensive cost of installation, and reliance on the weather for power output. The normal solar system efficiency ranges between 9% and 17%, taking into account the impact of various weather conditions.[3] Since solar power systems are weather-dependent, they are unreliable power sources. As a result, effective control mechanisms are needed to make sure the PV systems work well and safely.

Figure 1 display the nonlinearity of the P-V and I-V characteristics of PV with respect to module radiation and temperature. Unquestionably, a single spot on the P-V curve has been identified and named MPP, where PV cell produces maximum power. As a consequence, several distinct MPPT strategies for solar PV applications has been described under different environmental conditions.[4–6] There are two primary categories that can be used to classify solar MPPT algorithms: traditional and soft computing MPPT approaches. Traditional approaches are often utilised in a wide range of applications since they are simple and inexpensive to execute like perturb and observe (P&O), incremental conductance (INC), and so forth.[7–10] Even though P&O, and INC MPPT strategies are popular and work well when irradiance is uniform, they cannot track the MPP when irradiance changes quickly and there are partial shading conditions (PSC). These strategies also suffer from significant steady-state oscillations and poor convergence speed, which are their biggest problems. To counteract the frequent shortcomings of traditional approaches, MPPT strategies based on soft computing, like sliding mode control (SMC),[11] artificial neural network (ANN),[12] fuzzy logic control (FLC),[13] and metaheuristic-based approach (i.e., particle swarm optimization [PSO],[14] genetic algorithm,[15] etc.) developed. These computationally-based MPPT approaches are able to handle system nonlinearity in order to monitor the global MPP (GMPP), particularly under PSCs.[16–18] Despite this, the complexity and computational workload of soft-computing approaches remain the main challenges. As a result, the goal of this research is to create and implement a straightforward yet effective controller that can adapt to changing weather patterns and suppress the cutting-edge and traditional MPPT controller limitations.

1.2 | Current status of MPPT strategies

Numerous efforts have been committed by researchers to the development of these MPPT strategies to upgrade the SPV system response. A filter-based adaptive fuzzy proportional integral derivative (FPIDN)-MPPT suggested to improve the accuracy, efficiency, and tracking speed of SPV systems. The time required to accomplish MPP is 48 ms, and the efficiency is 99.45%–99.72%. Even so, this strategy requires recurrent optimization, which is time consuming and expensive.[19] For minimising oscillations and enhancing convergence speed without sacrificing the ease of implementation and simplicity

of fundamental INC and P&O approaches, a SOFT (Steady Output & Fast Tracking)-MPPT approach presented. Through experimental and simulation testing, it was shown that the method is more effective and adapts to a broad variety of loads. On the other hand, the effectiveness of strategy is only evaluated under constant weather circumstances, and the effect of PSC is ignored.[20] For a standalone SPV with a SEPIC converter, a load voltage-based approach (LVB) with customizable step size presented. The suggested strategy has faster convergence speed than the fixed step size scheme, P&O, and INC methods over a wide range of radiation circumstances. Unfortunately, the framework's robustness to temperature, load, radiation and PSC is not considered.[21]

To address the limitations of traditional sliding mode controllers (SMC) used for MPPT in solar power generation systems, a robust SMC presented. This research employs hysteresis quantized input (QI) to lessen the chattering problems while also providing additional advantages. The performance is evaluated exclusively in constant meteorological circumstances, and the effect of PSC is omitted.[11] A reduced oscillation-P&O (ROPO) strategy described to eliminate direction loss and oscillation. The strategy captures MPP in 0.018 s and has an efficiency range of 99.06%–99.80%. However, its performance under simultaneously varying radiation, load, temperature, and PSC variations has not been evaluated.[22] A simplified P&O approach with coarse and fine control is suggested. The method is not only easy to implement but also addresses all of the drawbacks of the traditional P&O, including inefficient tracking, excessive levels of oscillation, and wasted energy. However, the research does not elaborate on the controller's performance with PSC and grid integration.[23] A MPPT is presented using adaptive robust fuzzy proportional integral (ARFPI) technique. PSO was utilised to adjust the controller parameters by minimising an equal-weighted composition of integral time absolute error (ITAE) and integral absolute error (IAE). The result showed that the ARFPI controller was better (there were less undershoots and ripples).[24] To improve the functionality of PV systems, a variable step backstepping (VS-BS) MPPT introduced. Under radiation, load and temperature circumstances, the strategy can precisely record MPP with negligible overshoot and oscillation. But the recommended controller's efficacy in PSC and grid integration is left unexplored.[25]

A hybrid adaptive network based fuzzy inference system (ANFIS)-PSO based MPPT approach designed and implemented in zeta converter to provide quick and zero oscillation tracking. A space vector modulation hysteresis current controller is used as the inverter control approach to achieve high-quality inverter current by tracking a precise reference sine-shaped current. The suggested MPPT outperforms the ABC (artificial bee colony), P&O and ACO (ant colony optimisation) approaches in terms of providing fast, precise, and accurate PV tracking in varying weather situations. The ANFIS-PSO has an average power tracking efficiency of 98.35%, followed by the ABC with 97.11%, and the PSO with 94.88%. The suggested grid-integrated PV system verified experimentally using a MATLAB-interfaced dSPACE, and the results verify the perfect design of control algorithms.[26] Power optimization and dynamic performance in a grid-connected PV system were improved by the development of an intelligent fuzzy PSO (FPSO)-MPPT scheme and a redesigned space vector PWM-based ripple compensator controller. Zeta converters have reduced output ripple and efficient load voltage regulation. Under dynamic environmental conditions, the FPSO-MPPT provides superior tracking efficiency.[27] An adaptive TS-fuzzy RBF neural network (ATSFRBFNN)-based PV MPPT presented for grid-connected PV systems to produce the most effective duty to boost converter. With the help of the cutting-edge learning algorithm, PV power tracking is fast and precise even when the solar radiation changes. The proposed MPPT controller outperforms GA-RBF neural network and TS-fuzzy-MPPT in terms of recognition rate, resilience, and optimal PV power tracking across a wide range of environmental conditions. In partial shade conditions, the technique behaviour is examined, and it is found that precise GMPPT is accomplished with shortest tracking duration.[28] A hybrid simplified Firefly and neighbourhood attraction firefly (HSFNA)-MPPT approach invented, and it is used in the implementation of a high-power SEPIC converter powered by PV for ultra-fast charging systems. The HSFNA is capable of GMPPT in the presence of PSC and other dynamic operating situations; it also has faster tracking, more precise responses, and greater efficiency.[29] A new optimised orthogonal hybrid firefly based ant colony method (NOOHFACM)-MPPT approach proposed for PV system with water pumping applications. The approach outperformed ACO and firefly algorithms in terms of PV power and tracking speed under fluctuating weather circumstances. The functionality of the system is verified by practical validation utilising a dSPACE DS1104 interface.[30] For agricultural purpose in remote areas, a standalone PMSM drives-based PV pumping system with a modified firefly approach (MFA)-MPPT driven Luo converter implemented and analysed using the dSPACE platform. Extensive experimental comparisons between MFA, PSO and P&O, demonstrate that the MFA provides superior tracking performance with minimal complexity under erratic climate circumstances. The developed system has less complicated installation, zero maintenance, and effective control; it may be used in rural regions for agricultural uses under varied solar insolation levels.[31] A novel continuous mixed p-norm (CMPN) based adaptive asymmetrical FLC (AAFLC) approach for inverter control strategy of single phase grid connected PV systems is presented. In this case, non-linear properties of the PV module are compensated by using asymmetrical membership functions, which results in a significantly enhanced

system. A comprehensive practical analysis provided to validate the efficiency of the suggested inverter controller design in a range of environmental conditions.[32]

1.3 | Methodology and key contributions

As per the literature survey, it is noticed that none of the article verified MPPT performance under diverse atmospheric conditions such as simultaneously varying irradiance, temperature, and load; partially shaded with 3×1 PV string and grid integrated with cloudy weather conditions. Additionally, the existing MPPT approach that address the issue of multiple peaks do not take into account the probability of tracking failures caused by the dynamic radiation changes. These facts have motivated the authors to design a novel hybrid two-stage MPPT structure for SPV system. The first stage is based on P&O control law, followed by the modified MRAC in the second stage. The conventional MRAC used in the literature is focused at first-order systems and its performance is inadequate under diverse situations. The majority of the plants, including PV system with boost converter are second-order system. Hence, the control law is derived by modifying conventional MRAC, that is, MMRAC for MPPT application. The key benefits of the proposed MPPT approach include rapid tracking response, reduced power fluctuations, and minimum losses. Following are the significant contributions of this work.

1. A simple and efficient MMRAC controller is presented for optimal MPPT in the SPV system.
2. The recommended approach's findings are thoroughly compared with those of traditional and cutting-edge MPPT methods including ANFIS, INC, VSPO and P&O.
3. Being adaptive, MMRAC is robust to simultaneously changing radiation, load and temperature levels.
4. The recommended controller robustness is also verified under partially shaded with 3×1 PV string and complex shading with dynamic irradiance change.
5. The three-phase 50 KW grid-connected PV system is verified under changing radiation without and with two cloud effects.
6. Real-time verification with the OPAL-RT simulator (OP4510) further demonstrates the practicability of the suggested strategy.

Based on aforementioned plan, a structured methodology is presented in the Figure 2 to discovering robust MPPT strategy for SPV system. The PV system description is presented in Section 2. The background information and system explanation are provided in Section 3. The recommended controllers detailed methodology is outlined in Section 4. Section 5 presents the simulation and experimental results and analysis. Finally, the study finishes with a brief conclusion of its key points.

2 | DESCRIPTION OF PV SYSTEM

Figure 1 demonstrates I-V & P-V curve of a simulated PV array in changing meteorological conditions.[33] It was tested with radiation levels ranging from 0.4 to 1 kW/m^2. The MPP is generated at the knee of the curve (maximum current [I_M] and maximum voltage [V_M]). Transmission of electricity from the PV system to the load is accomplished with the help of a boost converter, and its basic architecture is depicted in Figure 3.

In v_{pv} and i_{pv} denotes the PV array voltage and current, respectively; L_{01}, C_0, and C_i are inductance, output and input capacitance of the boost converter, respectively. The goal is to create an MPPT controller that continuously determines the optimal duty cycle so that v_{pv} follows the trajectory of V_M and i_{pv} follows the trajectory of I_M, resulting in maximum possible available power. Here, a model consisting of a single diode was used for this investigation.

When the rate of change power w.r.t PV voltage is zero as visible in Figure 1, MPP occurs. This is shown mathematically in the form of Equation (1).

$$\frac{dp}{dv_{pv}}\begin{cases}=0, \text{at the MPP}\\ <0, \text{at the right side of the MPP}\\ >0, \text{at the left side of the MPP}\end{cases} \tag{1}$$

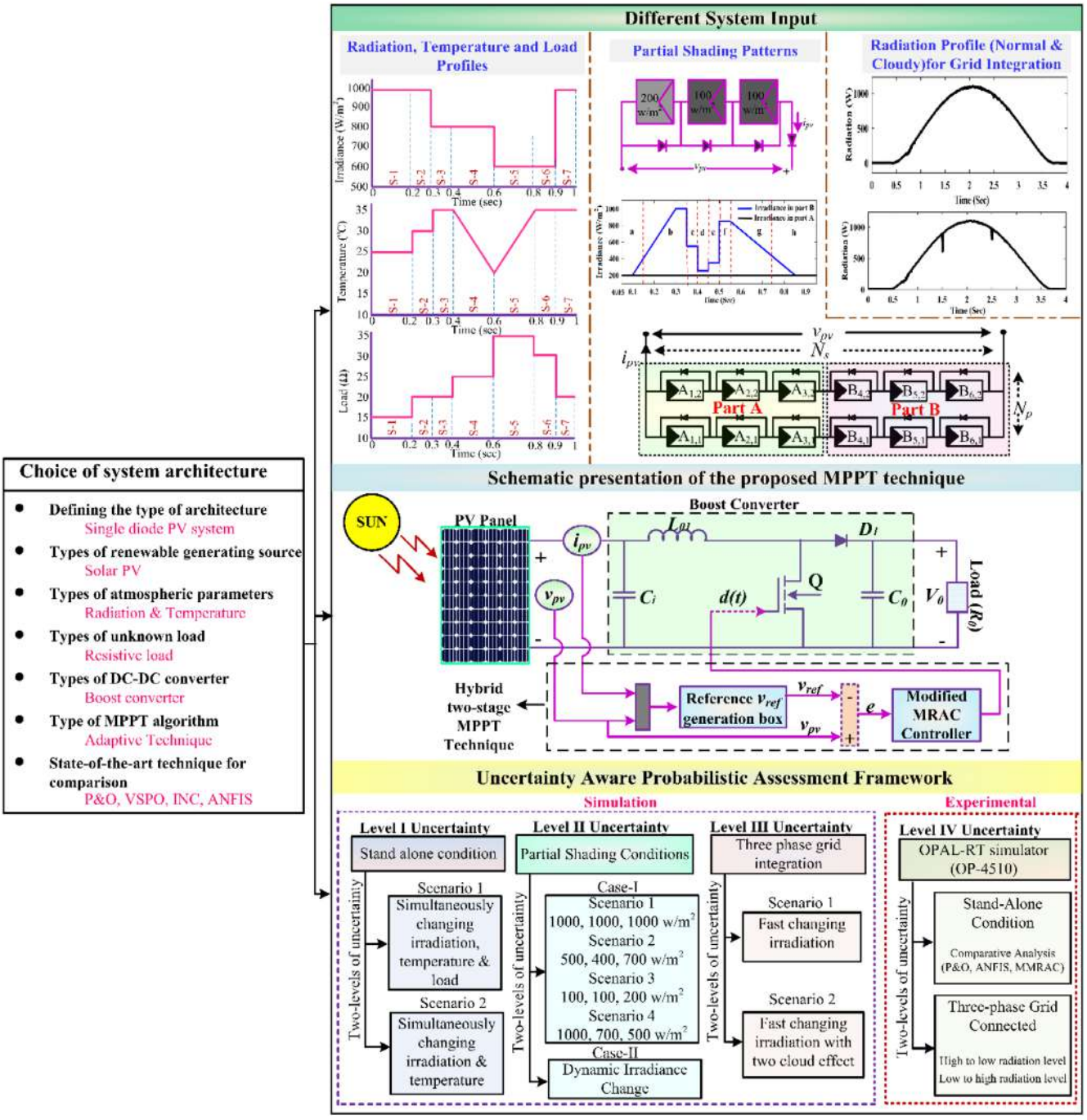

FIGURE 2 Schematic illustration of the methodology for recommended MPPT strategy.

3 | BACKGROUND WITH SYSTEM EXPLANATION

3.1 | PV system with boost converter

A simple PV system's current or voltage is controlled by a dc–dc converter connected to an MPPT controller in order to generate the most electricity, as seen in Figure 3. The MPPT controller translates the PV voltage (v_{pv}) and current (i_{pv}) from the PV panel into a duty cycle ($d(t)$) that controls the switching Q. Both the DC and ripple components contribute to the total PV voltage and current. The goal of MPPT method is to capture and transmit as much solar energy as feasible to load in order for v_{pv} and i_{pv} to follow V_M or I_M as shown in Figures 1 and 5.

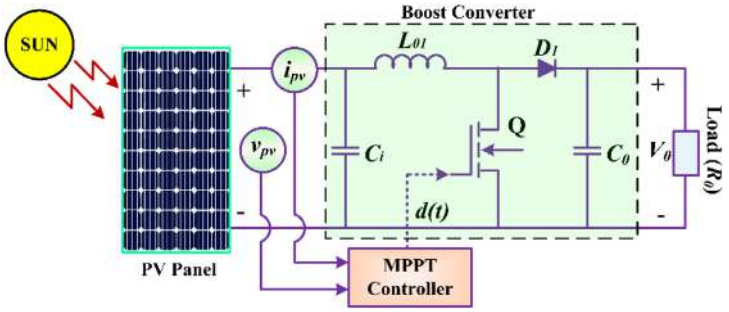

FIGURE 3 PV system with MPPT controller.

The steady-state relationship between the i_{pv}, v_{pv}, and $d(t)$ can be stated as:

$$v_{pv} = i_{pv}R_0(1-d)^2 \tag{2}$$

with $v_{pv} = V_{pv} + \hat{v}_{pv}$ & $i_{pv} = I_{pv} + \hat{i}_{pv}$. where I_{pv} & $\hat{i}_{pv}$ are PV array DC and ripple terms. V_{pv} & $\hat{v}_{pv}$ are PV voltage DC & ripple terms.

The boost converter operates according to the following relationship between its input voltage (v_{in}) and output voltage (V_0):

$$V_0 = \frac{v_{in}}{1-d} \tag{3}$$

Here v_{in} represents the input voltage with a value of 58 V. The converter is designed to provide an output voltage (V_0) of 128 V, which corresponds to a duty cycle (d) of 0.54 when Equation (3) is used. The MPP current, that is, $I_M = 14.7A$ is used as the input current (I_{in}) for the converter, and Equation (4) is used to calculate the output current (I_0), which is found to be 6.66 A.

$$I_0 = (1-d)I_{in} \tag{4}$$

To determine the value of inductance (L_{01}) for boost converter, Equation (5) is used. The ripple content in the output current is denoted as ΔI and is assumed to be 5% of I_0. The switching frequency (f_s) is set at 25 kHz, and the designed value of L_{01} is found to be 3.8 mH.

$$L_{01} = \frac{v_{in} * d}{f_s * \Delta I} \tag{5}$$

Equation (6) is used to determine the capacitance value (C_0) for the boost converter. The ripple content in the output voltage V_0 is denoted by ΔV and is assumed to be 2% of V_0. The designed value of C_0 is found to be 113.83 μF. The value of C_i is considered as 113.83 μF.

$$C_0 = \frac{I_0 * d}{f_s * \Delta V} \tag{6}$$

Using Equation (7), the load resistance R_0 is calculated to be 19.21 Ω based on the values of V_0 and I_0.

$$R_0 = \frac{V_0}{I_0} \tag{7}$$

Finally, Equation (8) is used to calculate $d(t)$. The value obtained is 0.54, where V_M and P_M represents the maximum voltage and maximum power, respectively.

$$d_{MPP} = 1 - \frac{V_M}{\sqrt{P_M * R_0}} = 0.54 \tag{8}$$

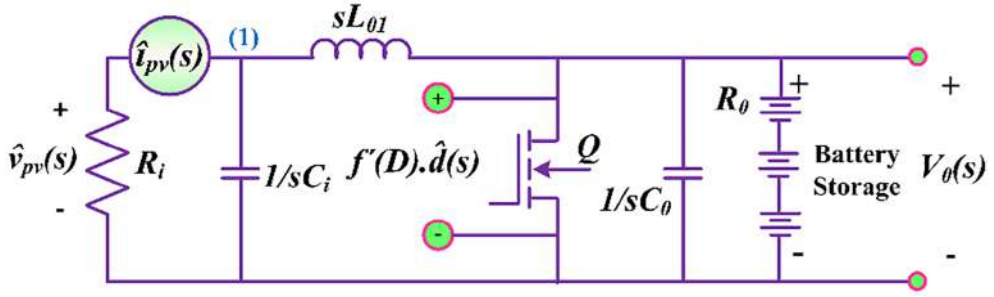

FIGURE 4 Small signal equivalent model of PV system.

3.2 | Small-signal modelling of SPV system

In steady state, the array voltage is related to the converter's duty cycle as shown in Equation (2). Therefore, MPPT control must consider the relation between duty cycle and array voltage if it is intended to optimise transient response. For the sake of clarity in the transient analysis, Figure 4 illustrates a small signal equivalent to Figure 3.[34]

As illustrated in Figure 4, $\hat{v}_{pv}(s)$, R_i and $\hat{i}_{pv}(s)$ stand for the small signal PV voltage, resistance and PV current, respectively. In small signal operation, the transfer function from the duty cycle to the array voltage is now formed around a functional point, neglecting the dynamics of the load, in this case the battery. The frequency-domain connection between $\hat{d}(s)$ and $\hat{v}_{pv}(s)$ is calculated as follows at node (1) using the KCL method:

$$\frac{\hat{v}_{pv}(s)}{R_i} + s\hat{v}_{pv}(s)C_i = \frac{f'(D)\hat{d}(s) - \hat{v}_{pv}(s)}{sL_{01}} \tag{9}$$

where $\hat{d}$ represents small signal fluctuation at the operational point, around the duty cycle D; Laplace transforms of $\hat{v}_{pv}(t)$ and $\hat{d}$(t) are $\hat{v}_{pv}(s)$ and $\hat{d}$(s) respectively; The boost converter steady-state input (V_{pv}) and output voltage (V_0) are correlated with the duty cycle (D), denoted by $f(D)$. The derivative of the duty cycle function $f(D)$ at the operational point D is denoted by $f'(D)$.

After rearranging the preceding equation, we get

$$\frac{\hat{v}_{pv}(s)}{\hat{d}(s)} = \frac{f'(D)}{L_{01}C_i s^2 + \frac{L_{01}}{R_i}s + 1} \tag{10}$$

It's well-known that

$$f(D) = V_{pv} = (1 - D)V_0 \tag{11}$$

In this case, it is assumed that Equation (11) is invariant under transient response. With respect to (11), we now have

$$f'(D) = -V_0 \tag{12}$$

Putting $f'(D)$ value from Equations (12) into (10), we obtained

$$\frac{\hat{v}_{pv}(s)}{\hat{d}(s)} = \frac{-\frac{V_0}{L_{01}C_i}}{s^2 + \frac{1}{R_iC_i}s + \frac{1}{L_{01}C_i}} \tag{13}$$

As the duty ratio decreases, the panel voltage increases, as indicated by the negative sign in Equation (13). The obtained transfer function in Equation (13) was estimated by linearizing (Figure 4) the nonlinear system shown in Figure 3, at a single operating location. When irradiance level shifts, the system operating location shifts and the corresponding Equation (13) value also changes, with the R_i being the most affected. The effect of R_i on the system may be evaluated by

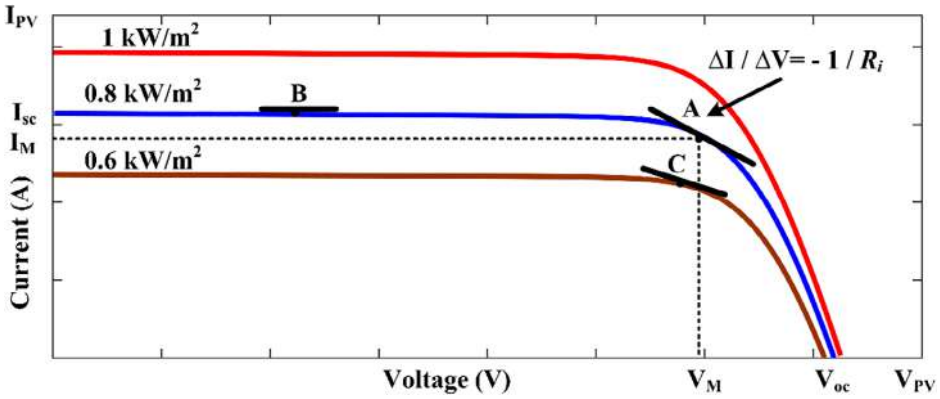

FIGURE 5 I-V curve with shifting R_i.

looking at Equation (13) denominator part.

$$s^2 + 2\xi\omega_n s + \omega_n^2 \tag{14}$$

where ω_n denote the natural frequency and ξ is damping ratio. When comparing the denominator of Equations (13) to (14), we see that

$$\xi = \frac{1}{2R_i}\sqrt{\frac{L_{01}}{C_i}} \text{ and } \omega_n = \frac{1}{\sqrt{L_{01}C_i}}$$

Underdamped system ($\xi < 1$) exhibit oscillations in response. Using an adaptive controller to regulate controlled plant dynamics can prevent under-damped fluctuations and other undesired behaviours. Controlled plants should be critically damped ($\xi = 1$) system (CDS). A CDS may be achieved at a single operating point by switching the R_i value, but it is not possible to maintain a critical damping system at all operating points with fixed R_i. Figure 5 depicts the I-V characteristics of a PV at three distinct degrees of solar insolation, particularly 600, 800, and 1000 W/m^2. The R_i is calculated based on slope tangential to system operating point.

$$\frac{1}{R_i} \approx -\frac{\Delta I}{\Delta V} \tag{15}$$

The MPP for the 800 W/m^2 curve is shown in Figure 5, denoted by A, that is, (V_M, I_M). R_i value at position A may be calculated from magnitude of the tangential line's inverse slope using the Equation (15). Moving the operating point from A to B with the same amount of solar insolation will obviously result in a different value for R_i. Furthermore, the MPP of 600 W/m^2 produces a distinct value of R_i when operating point is shifted from A to C. Thus, MPP switching does not promise that operational R_i will remain the same. The existence of a CDS is thus not assured by selecting the operational optimum R_i. As a result, a new model reference adaptive control strategy has been suggested in this paper to monitor MPP. The recommended strategy will be effective in achieving a CDS as well as optimise the converter dynamics. The following part demonstrates the proposed controller design.

4 | METHODOLOGY

Figure 6 depicts the MPPT Control Law (P&O) module as the starting point of control in the proposed strategy. This control module is responsible for providing a reference voltage (v_{ref}) for all MPP voltages. Next, the second step involves the implementation of the suggested MMRAC-MPPT controller. The MMRAC receives an input variable consisting of the difference in PV and reference voltage ($v_{pv} - v_{ref}$). The MMRAC provides a duty cycle to switch Q in order to maintain constant operation of PV panel at MPP.

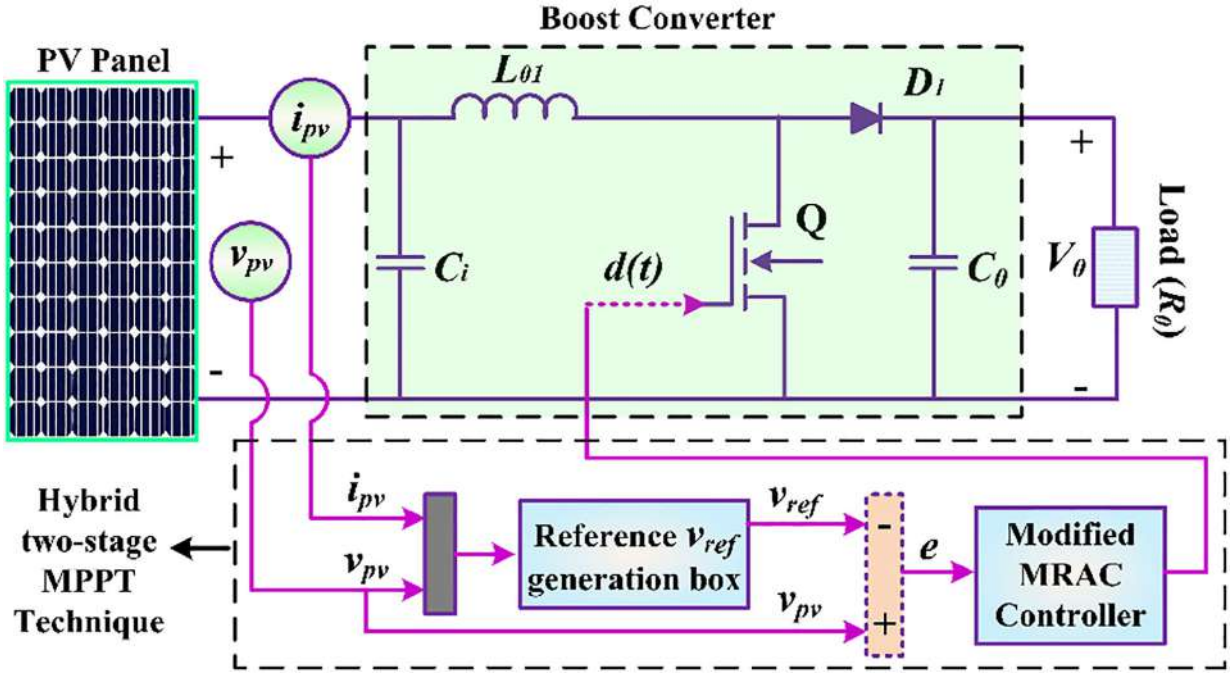

FIGURE 6 Illustration of the MPPT control architecture.

4.1 | MPPT control block (P&O)

The MPPT control law computing block provides v_{ref} for each MPP voltage. The control mechanism is currently being developed using a P&O technique. The MPPT control law discussed in Equation (1), where maximum power occurs and v_{ref} can change in accordance with the following formula. Where Δv is symbolised by small threshold voltage. Figure 7. depicts the suggested MPPT method's flowchart for generating v_{ref}.

$$v_{ref} = \begin{cases} v_{pv}, \frac{dp}{dv_{pv}} = 0 \\ v_{pv} - \Delta v, \frac{dp}{dv_{pv}} < 0 \\ v_{pv} + \Delta v, \frac{dp}{dv_{pv}} > 0 \end{cases} \tag{16}$$

4.2 | Proposed MMRAC approach

The P&O employed to calculate v_{ref} in the step before, which aims to provide maximum available power under steady-state conditions. Moreover, it is preferred that, upon experiencing a shift in solar insolation, the system rapidly converges to MPP. The MMRAC design's primary purpose is to keep the array voltage critically damped. The primary idea underlying MMRAC is to build an adaptive controller in such a way that the controlled plant response remains nearly identical to reference model response with the desired dynamics, even when uncertainties are present. The proposed MMRAC architecture is seen in Figure 8. It is the v_{ref} determined in Section 4.1 that serves as the input ($r(t)$) to the entire system.

Figure 8 plant model is equivalent to the transfer function seen in Equation (13). However, to simplify matters, we reverse its sign (multiply with -1) in order to have only positive coefficients in the plant model. Here, $u_p(t)$ and $y_p(t)$ denote plant input and output respectively. We considered a second order system since Equation (13) is a second order system.

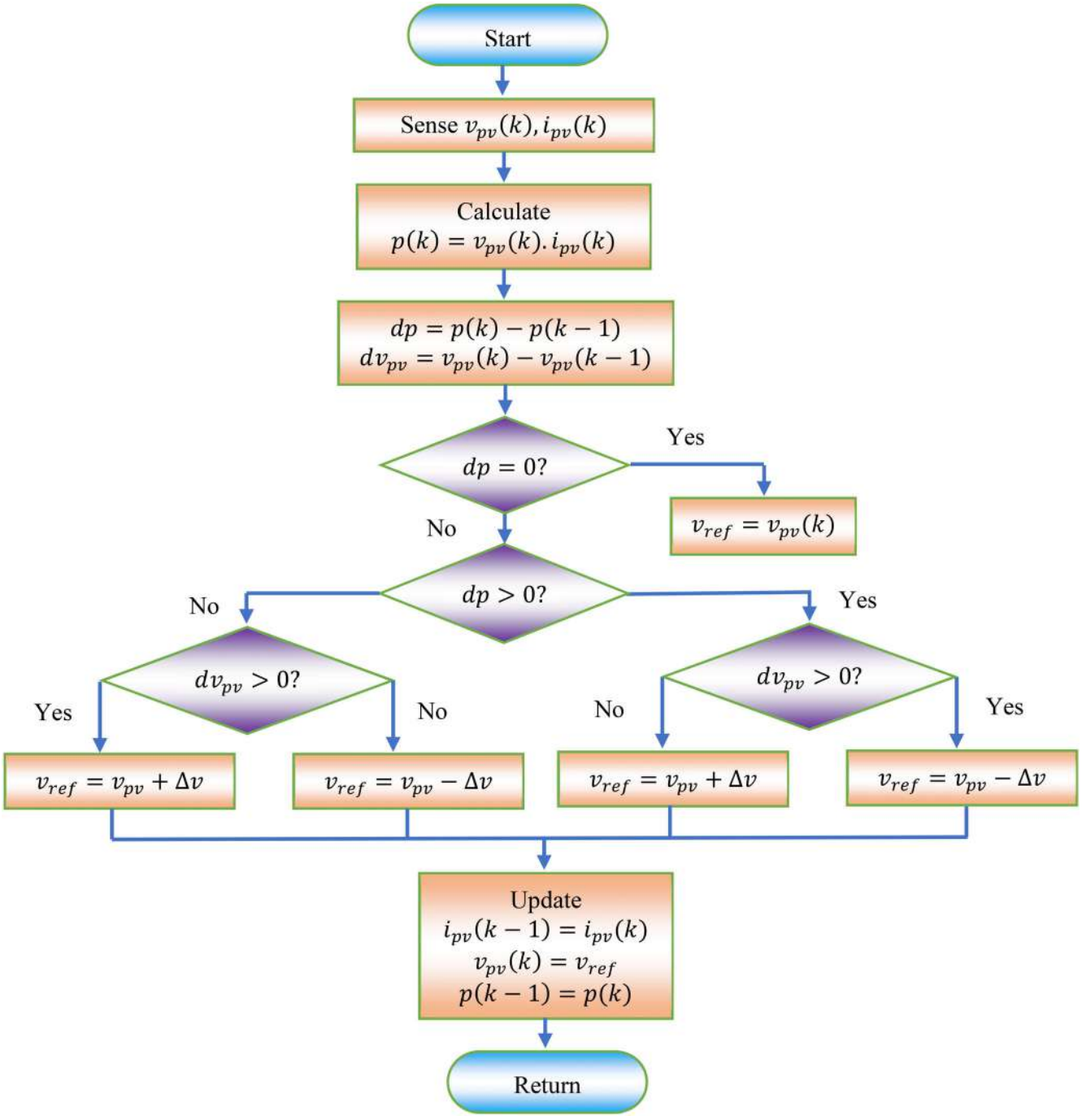

FIGURE 7 Flowchart for generating the reference voltage.

The following form, appropriate in both the time and frequency domains, was chosen as the second order plant model.

$$\frac{d^2y_p(t)}{dt^2} = -a_p\frac{dy_p(t)}{dt} - b_p y_p(t) + k_p u_p(t) \tag{17}$$

$$G_p(s) = \frac{y_p(s)}{u_p(s)} = \frac{k_p}{s^2 + a_p s + b_p} \tag{18}$$

where $a_p = 1/R_i \times C_i$, $b_p = 1/L_{01} \times C_i$ and $k_p = V_0/L_{01} \times C_i$ is plant parameter and it can be determined using Equation (13).

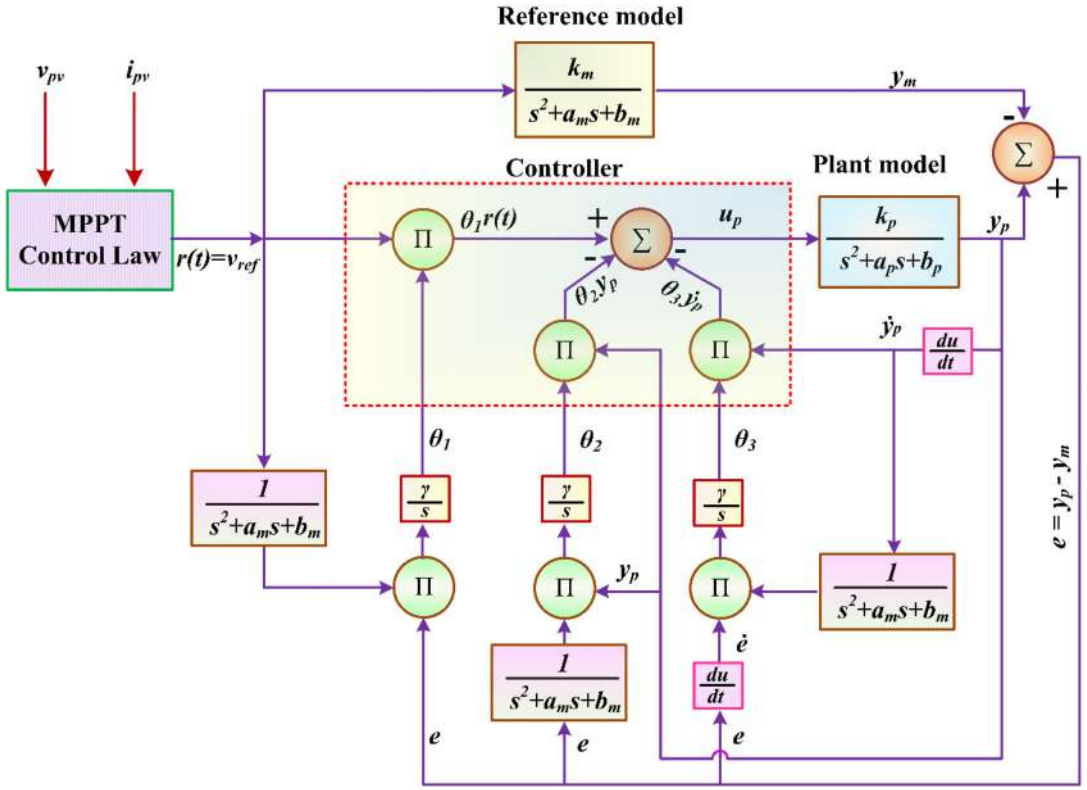

FIGURE 8 Controller structure in the proposed MMRAC.

The following form describes the relationship between the input $r(t)$ and the intended output $y_m(t)$ in the second order reference model (in both the time and frequency domains).

$$\frac{d^2y_m(t)}{dt^2} = -a_m\frac{dy_m(t)}{dt} - b_m y_m(t) + k_m r(t) \tag{19}$$

$$G_m(s) = \frac{y_m(s)}{r(s)} = \frac{k_m}{s^2 + a_m s + b_m} \tag{20}$$

where k_m represents positive gain, and b_m and a_m are calculated so that reference model generates a critically damped response. The goal of the control strategy is to develop $u_p(t)$ so that plant output ($y_p(t)$) follows reference model output ($y_m(t)$) asymptotically.

The parameters of the MMRAC controller's adaption law may be calculated using the MIT rule. According to MIT law, the cost function is formulated as below:

$$J(\theta) = \frac{e^2}{2} \tag{21}$$

$$e = y_p - y_m \tag{22}$$

The difference between plant (y_p) and reference model (y_m) constitutes the error that is denoted by e. The control parameter that can be adjusted is represented by the symbol θ. In order to achieve the goal of reducing the overall cost function to its minimum possible value, the value of the θ is adjusted using the MIT rule, which is given in Equation (21). As a result, we can write.

$$\frac{d\theta}{dt} = -\gamma\frac{\delta J}{\delta\theta} = -\gamma e\frac{\delta e}{\delta\theta} \tag{23}$$

where the terms γ and $\frac{\delta e}{\delta\theta}$ are used to describe adaptation gain and sensitivity derivative, respectively.

The controller architecture for accomplishing the targeted control goals is shown in Figure 8. The control law $u_p(t)$ is defined below for bounded reference input.

$$u_p = \theta_1 r - \theta_2 y_p - \theta_3 \dot{y}_p = \theta^T \varphi \tag{24}$$

where the estimated vector of controller parameter is denoted by $\theta = [\theta_1, \theta_2, \theta_3\ ]^T$and φ presents $\left[r, y_p, \dot{y}_p\ \right]^T$.

Substituting Equations (24) into (17), we get

$$\frac{d^2 y_p(t)}{dt^2} = -\left(a_p + k_p\theta_3\right)\frac{dy_p(t)}{dt} - \left(b_p + k_p\theta_2\right)y_p(t) + k_p\theta_1 r(t) \tag{25}$$

Comparing Equations (19) and (25) coefficient, we get

$$\theta_1 k_p = k_m \tag{26}$$

$$b_m = b_p + k_p\theta_2 \tag{27}$$

$$a_m = a_p + k_p\theta_3 \tag{28}$$

where θ_1, θ_2, and θ_3 are control parameters are converged as:

$$\theta_1 \approx \frac{k_m}{k_p}; \theta_2 \approx \frac{b_m - b_p}{k_p}; \theta_3 \approx \frac{a_m - a_p}{k_p} \tag{29}$$

Taking Laplace to transform in Equation (25), we get

$$\frac{y_p(s)}{r(s)} = \frac{k_p\theta_1}{s^2 + \left(a_p + k_p\theta_3\right)s + \left(b_p + k_p\theta_2\right)} \tag{30}$$

As per error Equation (22), we can write

$$e = \left(\frac{k_p\theta_1}{s^2 + \left(a_p + k_p\theta_3\right)s + \left(b_p + k_p\theta_2\right)} - \frac{k_m}{s^2 + a_m s + b_m}\right)r(s) \tag{31}$$

The sensitivity derivatives $\frac{\delta e}{\delta\theta_1}$, $\frac{\delta e}{\delta\theta_2}$ and $\frac{\delta e}{\delta\theta_3}$ are derived from Equations (31) to (30) given by

$$\frac{\delta e}{\delta\theta_1} = \frac{k_p r}{s^2 + a_p s + k_p\theta_3 s + b_p + k_p\theta_2} \tag{32}$$

$$\frac{\delta e}{\delta\theta_2} = \frac{-k_p y_p}{s^2 + a_p s + k_p\theta_3 s + b_p + k_p\theta_2} \tag{33}$$

$$\frac{\delta e}{\delta\theta_3} = \frac{-k_p y_p s}{s^2 + a_p s + k_p\theta_3 s + b_p + k_p\theta_2} \tag{34}$$

Considering $s^2 + a_m s + b_m = s^2 + a_p s + k_p\theta_3 s + k_p\theta_2 + b_p$. In Equation (23), the $\frac{\delta e}{\delta\theta}$ are replaced in accordance with the MIT rule (Equations 21 and 23). After restructuring, the Equations (35), (36), and (37) are employed to modify control parameters θ_1, θ_2, and θ_3 respectively.

$$\frac{d\theta_1(t)}{dt} = -\gamma\left(\frac{1}{s^2 + a_m s + b_m}r(t)\right)e(t) \tag{35}$$

$$\frac{d\theta_2(t)}{dt} = \gamma\left(\frac{1}{s^2 + a_m s + b_m}y_p(t)\right)e(t) \tag{36}$$

$$\frac{d\theta_2(t)}{dt} = \gamma\left(\frac{1}{s^2 + a_m s + b_m}\dot{y}_p(t)\right)\dot{e}(t) \tag{37}$$

Now that the MMRAC controller design has been finalised, and the outcomes are given in subsequent section.

5 | RESULTS AND DISCUSSION

A MATLAB/SIMULINK software was used to test the suggested controller's performance. In Figure 2, the suggested strategy's robustness to various levels of uncertainty is demonstrated. All of the simulation settings for the recommended strategy are detailed in Table 1. Error for five distinct methods were calculated using the following formula.[35]

$$\text{Mean absolute error (MAE)} = \frac{\sum |Estimated\ Value - Actual\ Value|}{n} \tag{38}$$

5.1 | Level-I uncertainty (stand-alone condition)

5.1.1 | Simultaneous variation in temperature, radiation and unknown load

The variation in irradiance, temperature and unknown load are depicted in Figure 9A–C, respectively. For every signal, there are seven distinct states. Day-to-day temperature and irradiance fluctuation have an impact on all of the recognised

TABLE 1 Parameters for simulation.

Parameters	Value	Parameters	Value
Open-circuit voltage (V_{oc})	36.3 V	Number of series module	2
Short-circuit current (I_{sc})	7.84 A	a_m	3.039×10^3(rad/s)
Rated current (I_M)	7.35 A	k_m	2.95×10^8 V (rad/s)^2
Rated voltage (V_M)	29 V	b_m	2.31×10^6(rad/s)^2
Rated power (P_M)	213.15 W	γ	0.08
Cells per module	60	a_p	351.40 (rad/s)
R_i	25 Ω	k_p	2.95×10^8 V (rad/s)^2
Number of parallel modules	2	b_p	2.31×10^6(rad/s)^2

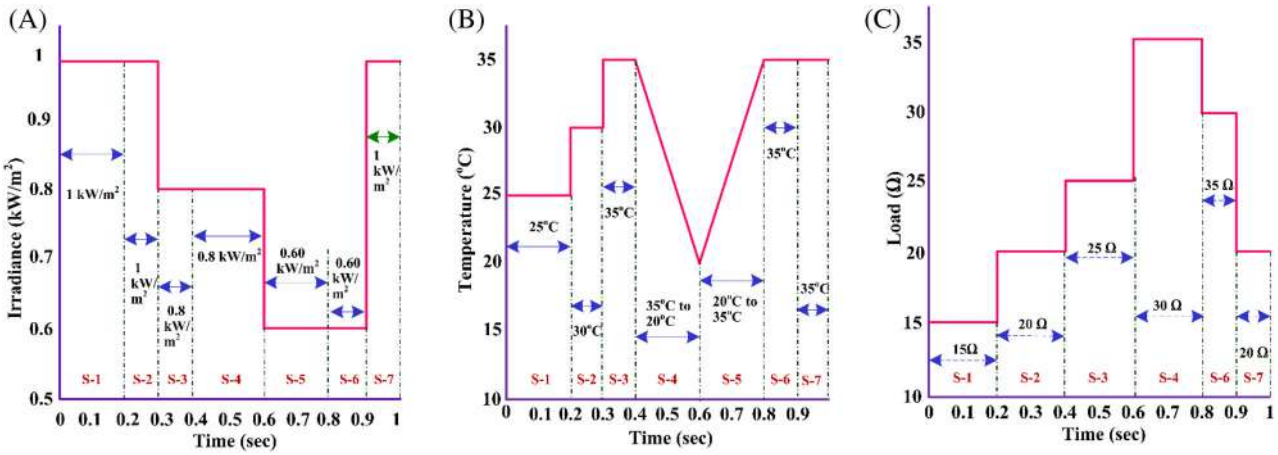

FIGURE 9 (A) Irradiation (B) Temperature (C) Unknown load sequence.

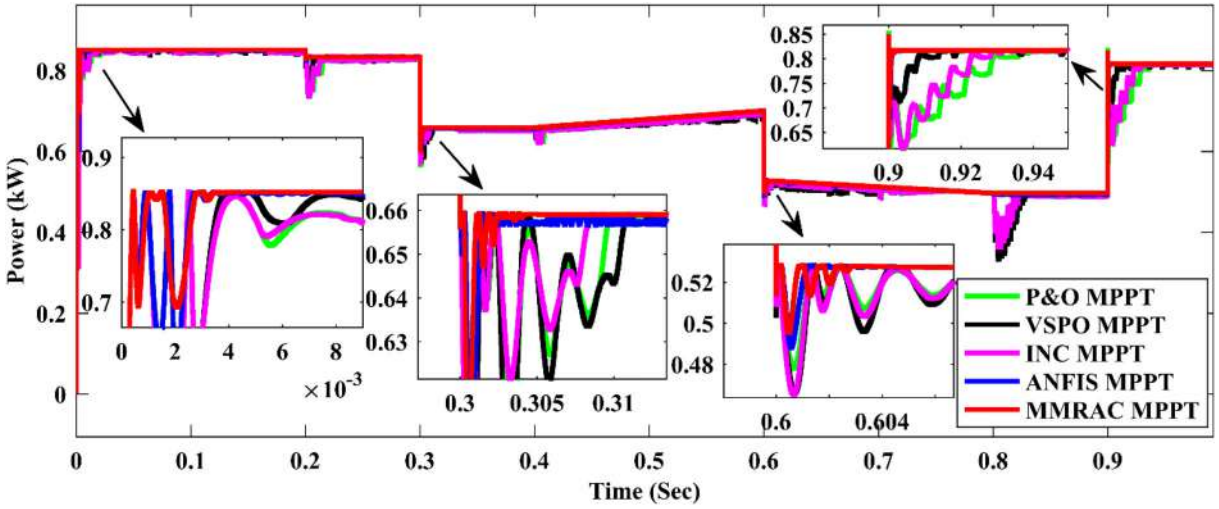

FIGURE 10 The PV power of five distinct MPPT strategies under changing load, temperature and irradiance.

states. PV systems with changing load resistance were anticipated to cause random perturbation in system. Figure 10 displays power from PV array using five distinct MPPT strategies while load, temperature and radiation change simultaneously. With respect to convergence speed, power loss, power output, efficiency, and error rates, the new MPPT worked admirably under all possible states of variation as shown in Table 2.

Various MPPT methods and their respective speeds are compared in Figure 11. As compared to ANFIS (0.021 s), VSPO (0.16 s), INC (0.20 s), and P&O (0.20 s), the novel method captures MPP in just 0.0038 s. Thus, the new MPPT method is the fastest for harvesting MPP. The INC, VSPO and P&O strategies have the largest ripple content around the MPP, which is minimised in ANFIS but at the cost of not being able to accomplish the MPP, and it is nearly zero for the proposed scheme which also allows for simple tracking of MPP across all seven states of the system.

Voltage & current ripple, convergence time, tracking efficiency, and power loss are graphically represented in Figure 12A–D, respectively, for five distinct MPPT strategies over seven states. The power loss (p_{loss}) is quantified by Reference 22:

$$p_{loss} = \frac{\sum p_{max}(t) - \sum p_{pv}(t)}{\sum p_{max}(t)} \tag{39}$$

where p_{max}, p_{pv} and t denote actual PV power, maximum power, and convergence time respectively. The recommended MPPT strategy produces the least amount of power loss, as illustrated in Figure 12D, when compared to other strategies. This indicates that, across all states, the suggested strategy has the lowest power loss and best tracking efficacy while also eliminating oscillations entirely.

5.1.2 | Simultaneous variation in radiation and temperature

Figure 9A displays the irradiance signal and Figure 9B displays the temperature signal. Figure 13 displays power from PV array using five distinct MPPT strategies while temperature and radiation vary simultaneously. Figure 14 shows that P&O approach requires maximum time to follow MPP at 100 ms followed by INC requires 70 ms, VSPO requires 50 ms, ANFIS requires 7 ms while the recommended strategy requires 3.7 ms. All seven states of MPP can be easily tracked using a proposed technique, which has very less ripple content around the MPP compared to the other techniques.

The INC, P&O, and VSPO strategies have ripple content, whereas ANFIS has low and the suggested strategy has insignificant ripple content. Convergence times for states 1–7 of the P&O scheme are 100, 43, 30, 37, 16, 10, and 42 ms. The INC scheme has a convergence time of 70 ms in state 1, 34 ms in state 2, 25 ms in state 3, 29 ms in state 4, 15 ms in state 5, 11 ms in state 6, and 34 ms in state 7. In case of VSPO scheme convergence time are 40, 30, 23, 26, 14, 20 and 15 ms in states 1 to 7 respectively. In case of ANFIS scheme convergence times are 7, 4, 8, 8.9, 5, 4.2 and 5.8 ms in states 1 to 7 respectively.

TABLE 2 Details assessment of five schemes including 7 states.

MPPT Approaches	S-1	S-2	S-3	S-4	S-5	S-6	S-7
Current ripple (A)							
P&O	0.96	1.10	0.94	1.14	0.89	0.80	0.83
INC	0.92	1.10	0.93	1.14	0.91	0.81	0.80
VSPO	0.75	0.89	0.71	1.10	0.81	0.71	0.50
ANFIS	0.31	0.061	0.039	0.041	0.059	0.059	0.079
MMRAC	0.030	0.04	0.019	0.019	0.020	0.031	0.039
Voltage ripple (V)							
P&O	3.17	3.84	3.47	4.71	4.61	3.72	1.81
INC	2.86	3.83	3.46	4.48	4.42	3.98	1.61
VSPO	2.50	3.32	3.17	4.51	4.10	2.82	1.21
ANFIS	0.98	0.31	0.31	0.41	0.49	1.39	0.038
MMRAC	0.15	0.12	0.02	0.081	0.059	0.48	0.019
Average actual power (W)							
P&O	821.2	829.1	654.8	663.7	495.8	492.7	815.2
INC	821.2	829.1	654.7	663.7	495.8	492.8	815.2
VSPO	825.6	829.8	654.8	664.6	498.4	495.5	817.0
ANFIS	846.7	842.8	664.2	671.2	503.9	500.4	825.2
MMRAC	851.7	851.4	679.6	681.2	508.6	511.0	851.6
Convergence time (ms)							
P&O	200	100	100	200	780	100	89
INC	200	100	100	200	758	100	70
VSPO	160	100	100	190	748	100	65
ANFIS	21	6.2	40	70	14	14	5.6
MMRAC	3.8	5.3	5	6	6.4	8.1	3.9
Average power output (W)							
P&O	809.2	806.4	649.3	646.2	479.3	480.1	809.7
INC	809.2	806.4	649.4	646.1	479.3	480.2	809.7
VSPO	816.3	813.6	656.2	656.1	481.2	483.7	815.1
ANFIS	829.9	828.2	665.1	662.4	494.3	496.5	827.4
MMRAC	843.1	843.1	667.9	668.8	502.0	506.1	842.5
Tracking efficiency (%)							
P&O	97.55	97.33	96.02	97.80	97.70	96.51	96.70
INC	97.55	97.33	97.12	97.80	97.70	97.50	97.70
VSPO	98.62	98.35	98.26	98.05	98.70	98.74	98.68
ANFIS	99.04	99.01	98.74	99.16	99.50	98.68	99.07
MMRAC	99.96	99.93	99.70	99.78	99.81	99.07	99.88

TABLE 2 (Continued)

MPPT Approaches	S-1	S-2	S-3	S-4	S-5	S-6	S-7
Power loss (%)							
P&O	3.49	2.45	3.66	2.39	2.69	3.39	4.21
INC	3.49	2.45	3.67	2.39	2.68	3.40	4.21
VSPO	2.98	2.48	3.63	2.33	2.50	3.07	4.10
ANFIS	0.62	1.07	2.55	1.53	1.41	2.11	3.14
MMRAC	0.04	0.07	0.29	0.03	0.50	0.03	0.04
Overall efficiency (%)							
P&O	95.69	95.27	95.47	95.05	95.00	95.25	95.62
INC	95.69	95.27	95.48	95.04	95.00	95.25	95.62
VSPO	96.73	96.38	96.70	96.81	96.11	96.58	96.71
ANFIS	97.99	97.81	97.72	97.30	97.11	97.59	97.75
MMRAC	98.89	98.85	98.04	98.29	98.11	98.84	98.81
MAE							
P&O	30×10^{-4}	217×10^{-4}	256×10^{-4}	171×10^{-4}	130×10^{-4}	172×10^{-4}	356×10^{-4}
INC	30×10^{-4}	217×10^{-4}	257×10^{-4}	170×10^{-4}	130×10^{-4}	171×10^{-4}	356×10^{-4}
VSPO	27×10^{-4}	217×10^{-4}	247×10^{-4}	166×10^{-4}	120×10^{-4}	156×10^{-4}	340×10^{-4}
ANFIS	4×10^{-4}	176×10^{-4}	232×10^{-4}	155×10^{-4}	90×10^{-4}	148×10^{-4}	251×10^{-4}
MMRAC	2×10^{-4}	155×10^{-4}	123×10^{-4}	134×10^{-4}	30×10^{-4}	119×10^{-4}	140×10^{-4}

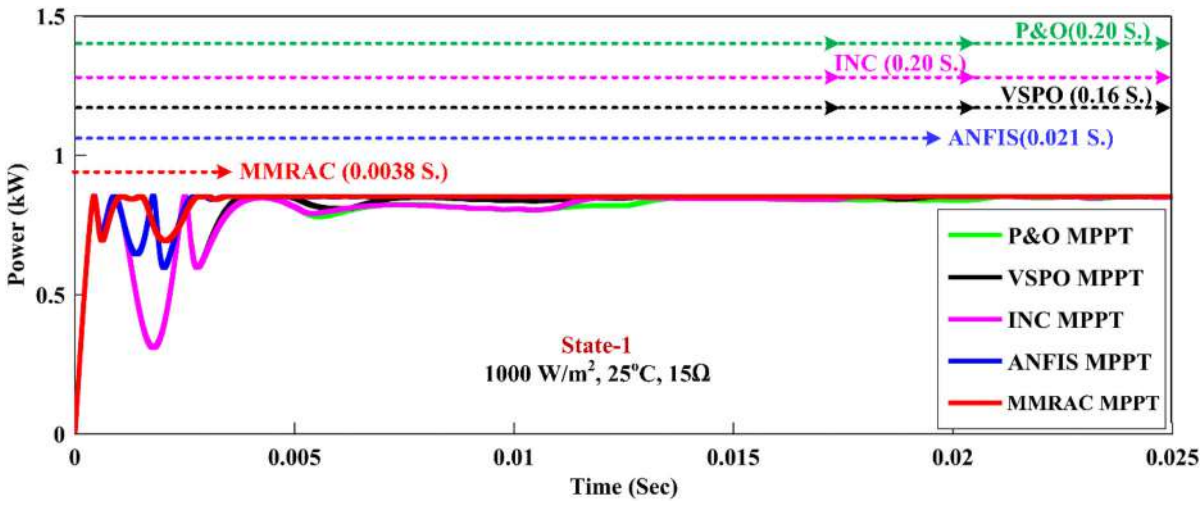

FIGURE 11 MPPT approach convergence speed under varying load, irradiation and temperature.

By taking into account the new method, the times required to follow MPP are extremely quick. The figures for state 1 to 7 are as follows: 3.7, 3.3, 4, 5.4, 3, and 3.7 ms. The P&O has a tracking efficiency of 95.81%–98.48%, for INC technique it is between 95.83% and 98.46%, and for VSPO technique 95.81%–98.66%, for ANFIS technique 96.05%–99.66%, whereas for the proposed technique it is between 97.10% and 99.96%. Figure 15 displays a visual representation of recommended strategy's superiority. For state 1, Figure 15 shows comparisons of the convergence time, tracking efficiency, voltage and current ripple over a web diagram.

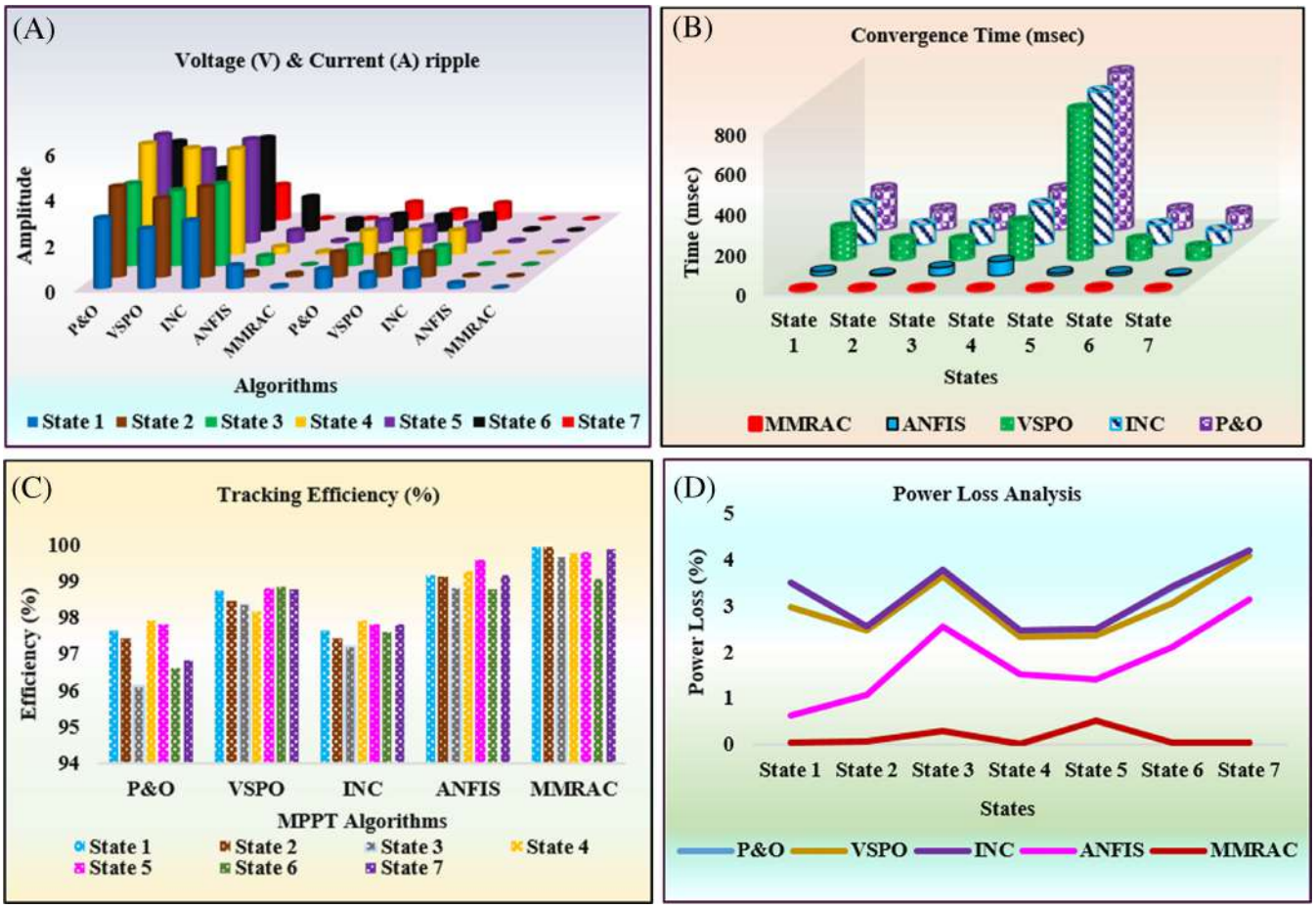

FIGURE 12 Performance comparison (A) voltage& current ripple (B) convergence time (C) tracking efficiency (D) power loss.

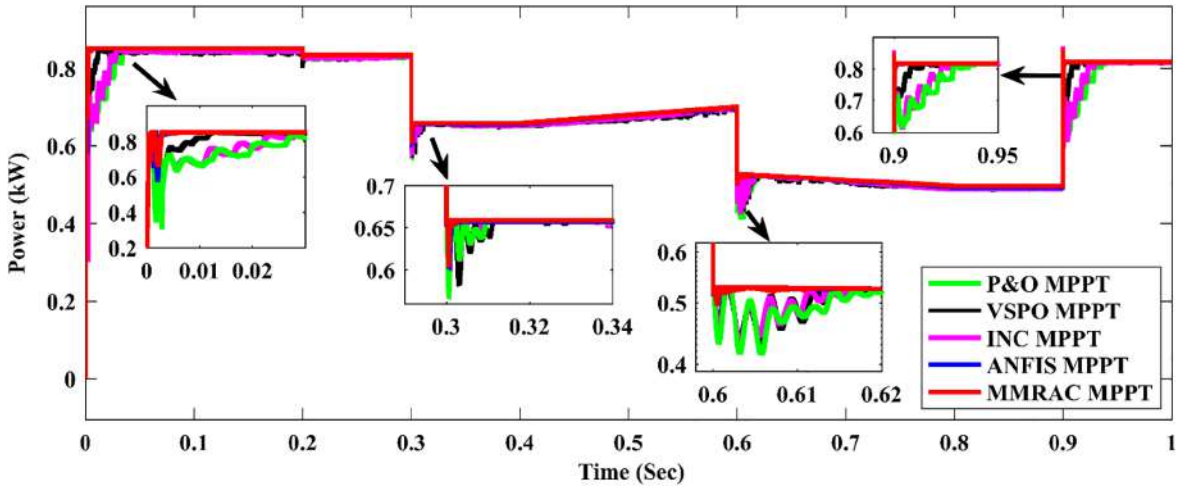

FIGURE 13 The PV power using five distinct MPPT strategies under changing temperature and irradiation.

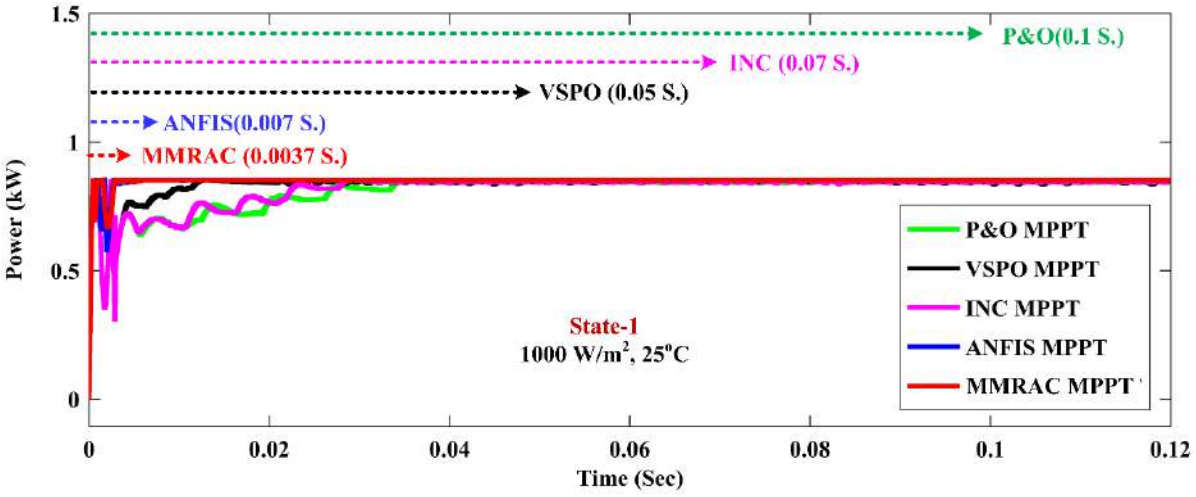

FIGURE 14 MPPT approach convergence speed under varying irradiation and temperature.

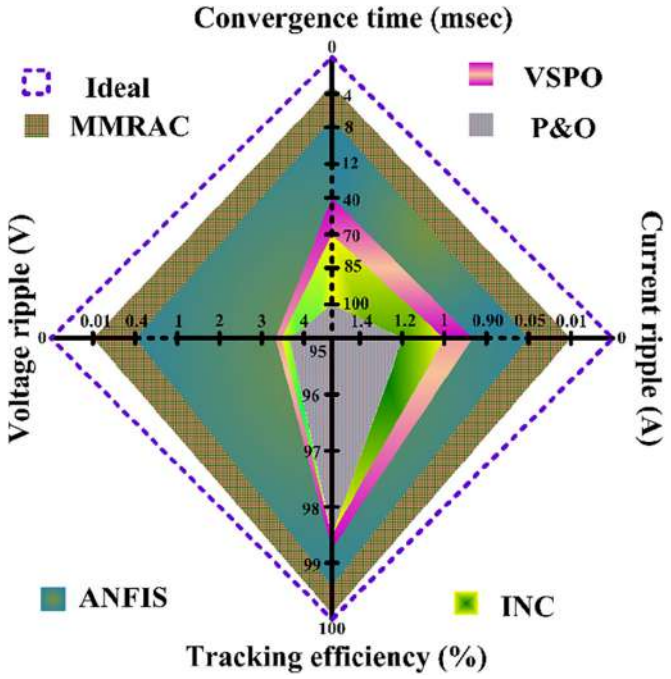

FIGURE 15 Visualisations indicating the advantages of the proposed strategy (A) voltage ripple (B) current ripple (C) convergence time (D) tracking efficiency.

5.2 | Level-II uncertainty

5.2.1 | Partial shading condition

Case-I

The proposed MPPT strategy is utilised to track the maximum possible power under PSC for a stand-alone system. The controller's functionality was evaluated in comparison to the ANFIS and P&O under four distinct shading circumstances. Furthermore, the effectiveness of suggested strategy has been assessed and compared using performance indicator such as shading losses and GMPPT. Even though PV technique has been advanced, partial shade still has an adverse effect on system and causes power loss. Shading loss is the difference between the maximum power output

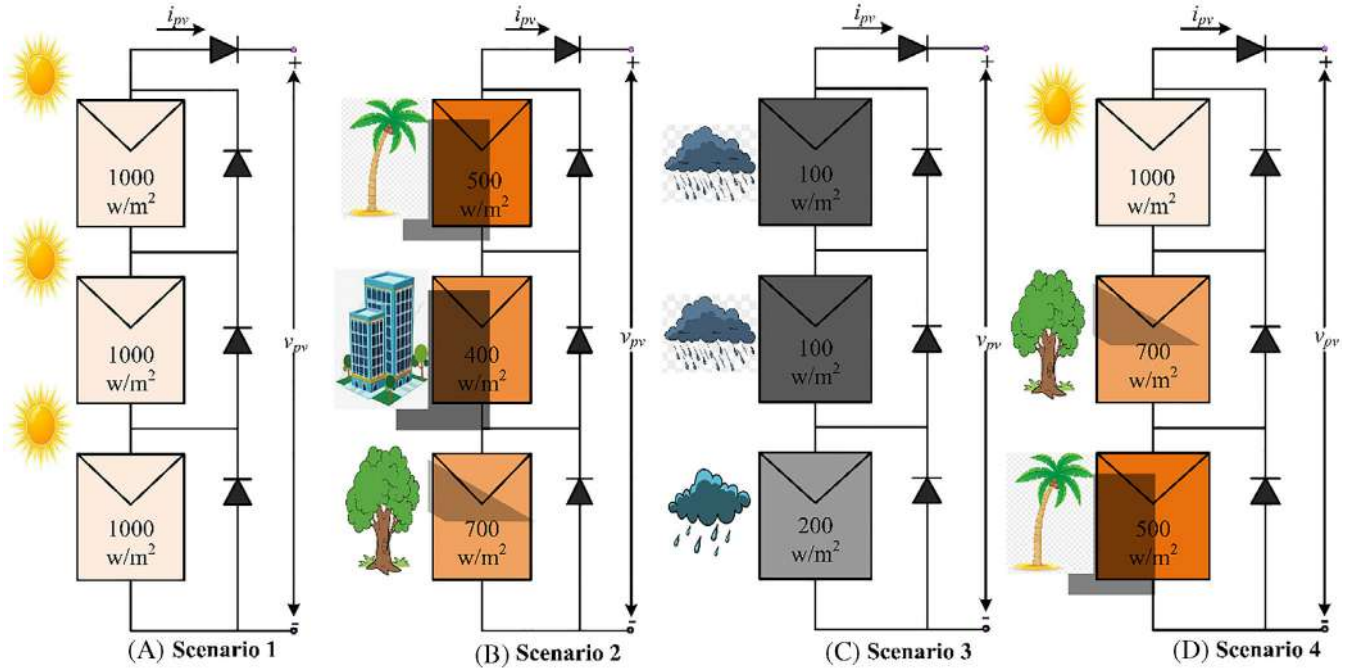

FIGURE 16 PV modules shading patterns.

measured in PSC ($p_{\text{mpp,without shading}}$) and that measured in STC ($p_{\text{mpp,shading}}$).[17] In mathematical terms, this is represented by the following Equation (40):

$$p_{\text{mpp,shading loss}} = p_{\text{mpp,without shading}} - p_{\text{mpp,shading}} \tag{40}$$

In the current investigation, the highest power output of the proposed system is 1.05 kW, achieved by connecting three PV modules in series. As can be seen in Figure 16, by exciting the modules with varying levels of irradiation, a wide range of shading effects may be achieved. The suggested stand-alone PV system's P-V curve under distinct shading circumstances are illustrated in Figure 17. Table 3 shows the local maximum power point (LMPP) and global maximum power point (GMPP) rates under different shading arrangements.

The shading patterns are thought to be at various GMPP peaks, such as the first, second, and third peaks. Figure 17 illustrates PV power with ANFIS, P&O, and MMRAC strategies under distinct irradiation arrangements. Table 4 provides the detailed steady-state performance of three distinct MPPT approaches under four PSC scenarios. Table 5 displays the corresponding shading losses.

Tables 4 and 5 demonstrate that the suggested strategy achieves maximum power with minimum shading loss in four distinct shading arrangements. However, in all four cases, the typical P&O strategy captures the least possible maximum power at the expense of the most significant shading loss. Furthermore, Figure 17 shows that the output of the P&O algorithm exhibits considerable perturbations. Figures 18 and 19 show the outcomes of a comparative examination of tracking power and shading loss for three strategies across four case studies.

Case-II

The PV array power-voltage curve can take on complex multi-peak shapes when affected by local shading, presenting a challenge for MPPT algorithms. However, many MPPT methods do not account for potential tracking failure that may arise due to changes in irradiance timing. The proposed hybrid MPPT approach is used to address MPPT failure caused by irradiance timing changes. The error between updated reference and PV voltage is used as input to MMRAC controller. The art of MMRAC lies in fitting appropriate controller parameters, which is achieved through identifying a suitable adaptive law. The proposed controller parameters are fine-tuned during adaption using the error between plant and reference model. Finally, the MMRAC block offers a reference signal for a duty cycle that is transmit into boost converter to guarantee that PV panel constantly operates at GMPP.

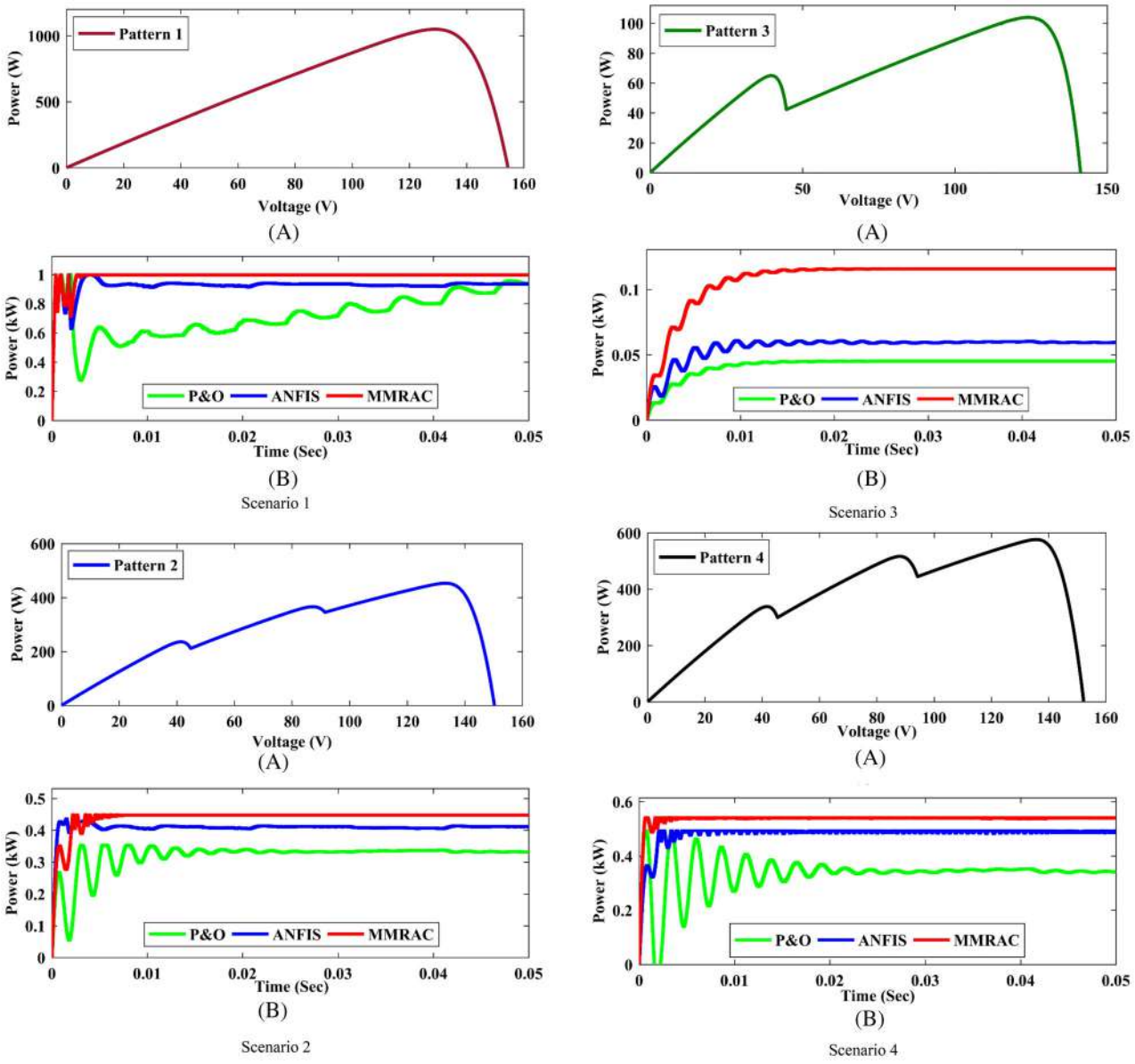

FIGURE 17 (A) P-V curves (B) PV power with ANFIS, P&O, and MMRAC techniques for different shading patterns.

TABLE 3 Power at LMPP and GMPP with four distinct shading arrangements.

	Scenario 1	Scenario 2	Scenario 3	Scenario 4
LMPP (W)	—	236, 366.1	65	338.2, 516.5
GMPP (W)	1049	453.3	124.1	576.4

Figure 20 illustrates the arrangement of the PV array into columns and rows. Region A is denoted by $A_{i,j}$ ($i = 1$–3; $j = 1$–2), while the other section is region B. The number of series connected solar cells (N_s) is 6 and the number of parallel-connected solar cell strings (N_p) is 2. The specifications of a single solar panel are listed in Table 1. The PV output characteristic curve for region A and B, which experience different lighting situations, is presented in Figure 21. It demonstrates how a change in the radiation condition of region B affects the MPP of the entire PV array if the irradiance of area A remains constant at 200 W/m^2. Figure 22A shows the irradiance signal of regions A and B.[36]

The irradiance might fluctuate gradually or dramatically during the simulation, as seen in Figure 22. Additionally, the MPP voltage amplitude frequently deviates, meaning that it continuously moves between right and left peaks as irradiance

TABLE 4 Steady-state behaviour of distinct MPPT strategies.

Shading scenario	Techniques	Power at MPP (W)	Voltage at MPP (V)	Current at MPP (A)
Scenario 1 (1000,1000,1000 W/m^2)	P&O	839.3	109.31	7.67
	ANFIS	929.4	113.20	8.21
	MMRAC	997.9	118.40	8.42
Scenario 2 (500, 400, 700 W/m^2)	P&O	333.1	69.10	4.82
	ANFIS	410.0	81.07	5.05
	MMRAC	447.9	82.79	5.41
Scenario 3 (100, 100, 200 W/m^2)	P&O	46.01	25.14	1.83
	ANFIS	60.00	35.50	1.69
	MMRAC	116.07	68.21	1.70
Scenario 4 (1000, 700, 500 W/m^2)	P&O	341.0	40.07	8.51
	ANFIS	491.2	59.76	8.22
	MMRAC	541.0	64.57	8.37

TABLE 5 Impact of shading loss (W) across distinct MPPT strategies.

	Pattern-1	Pattern-2	Pattern-3	Pattern-4
P&O	209.7	715.9	1002.99	708.0
ANFIS	116.6	639.0	989.00	557.8
MMRAC (Proposed)	51.1	601.1	932.93	508.0

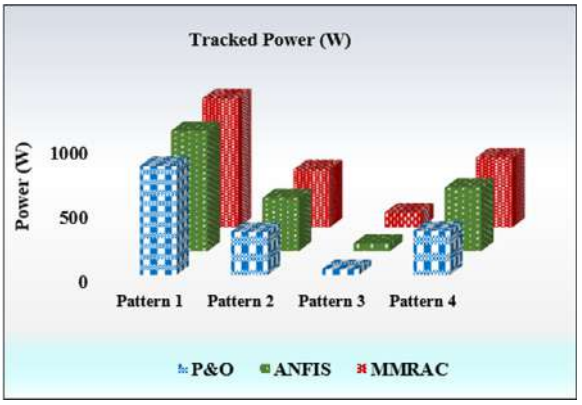

FIGURE 18 Comparative analysis of tracked power.

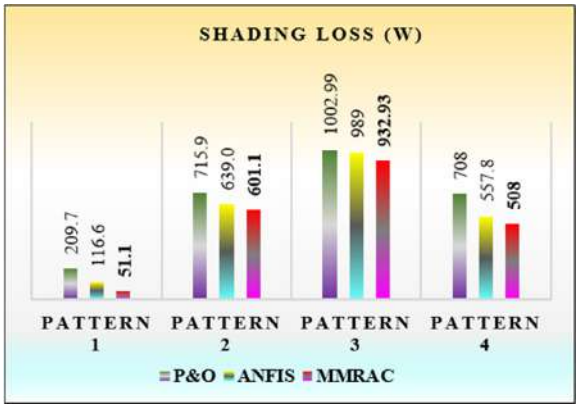

FIGURE 19 Comparative analysis of shading loss.

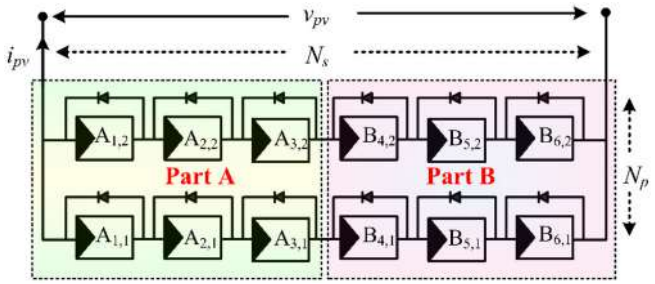

FIGURE 20 PV array model.

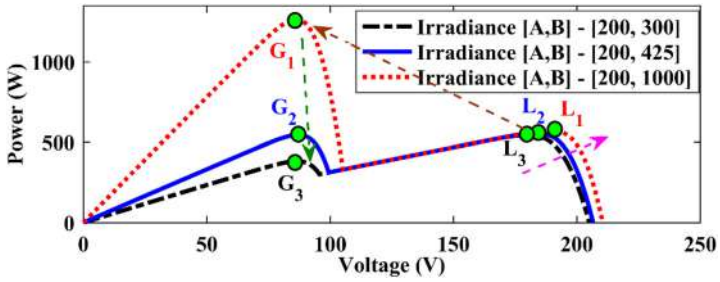

FIGURE 21 P–V curve of PV array under PSC.

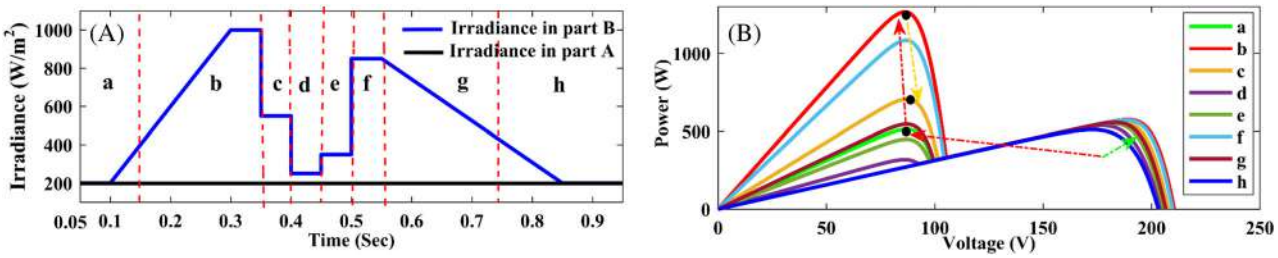

FIGURE 22 (A) Irradiances of distinct components of PV array (B) P-V curve.

shifts. The MPP may be found on the rightmost peak of the region labelled "a" in Figure 22A. Figure 22B shows that when the irradiance rises, the MPP progressively shifts to the left, reaching a peak at 0.16 s and then rising steadily thereafter. After 0.35 s, the MPP is still on the left peak, even though the irradiance has dropped from 1000 to 550 W/m^2. Area "d" of Figure 22 shows that when the irradiance is reduced from 550 to 250 W/m^2, the MPP on left peak moves to right peak at a time of 0.4 s. Figure 22A shows that at 0.45, 0.5, 0.55 and 0.74 s, the MPP moves from left peak to right peak alongside an accompanying change in irradiance.

The proposed controller can accomplish MPPT and prevent GMPPT failure regardless of variations in PV shading circumstances. The MPPT control effort emphasises PV system's output power, which is illustrated in Figure 23. The power generated by the PV array is a combination of the outputs from regions A and B. As depicted in the Figure 23 the suggested controller is highly efficient at achieving MPP and accurately follows the maximum power.

5.3 | Level-III uncertainty

5.3.1 | Three-phase grid integration condition

In two different scenarios, a 50 kW three-phase grid-connected PV system is simulated. Figure 24 depicts a MATLAB simulation of a grid-connected PV system and Table 6 contains the simulation parameters. A DC-DC converter and an

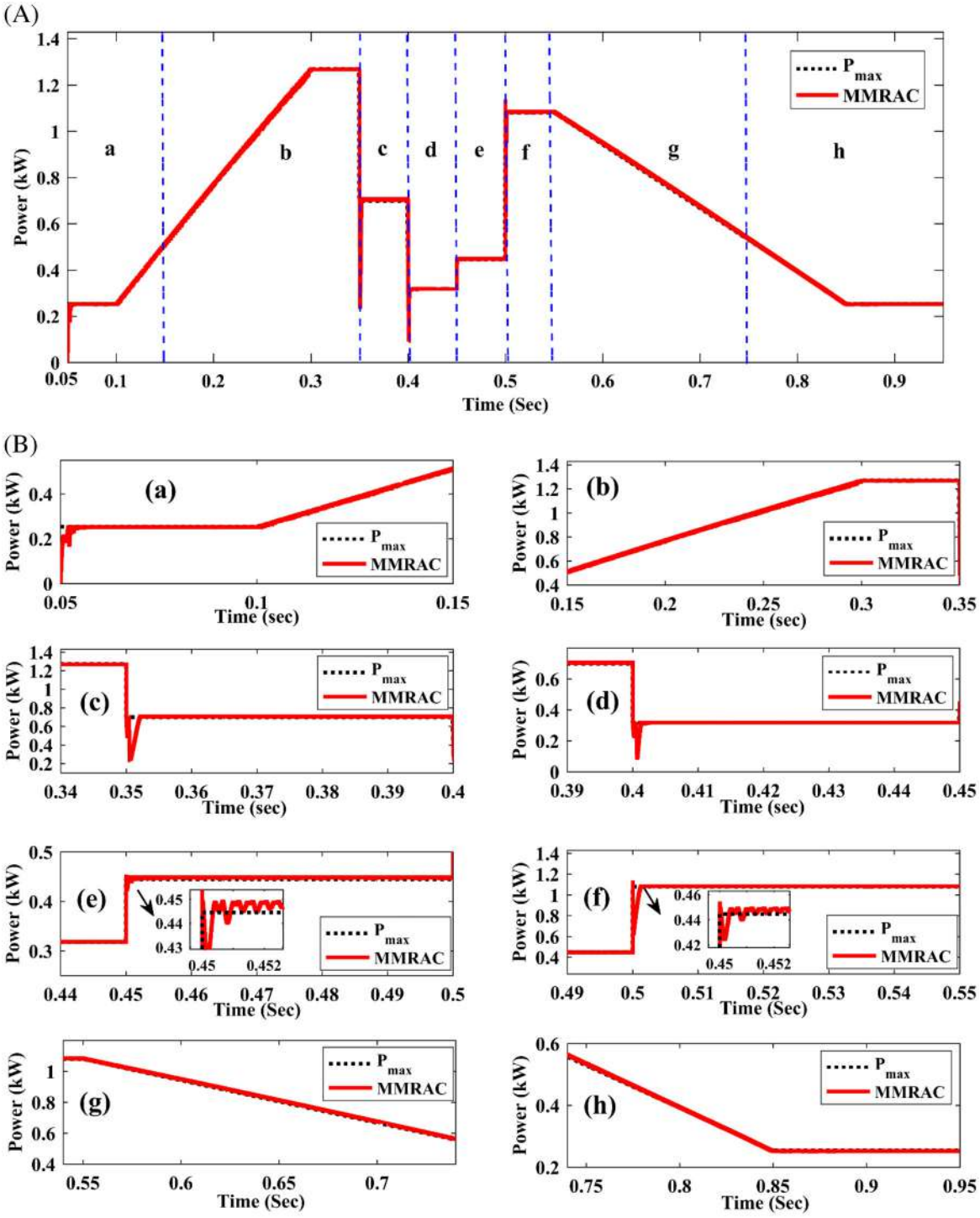

FIGURE 23 PV ideal and output power with MMRAC (A) overall output power (B) detailed output power.

inverter are used to connect the PV module to a three-phase network. The system is simulated in a variety of ways, including the following:

Scenario 1: Changing irradiation curve

Under two different radiation profiles, Figure 25. shows the simulation comparison between ideal PV power (p_{ideal}) and maximum achievable PV power (p). Figure 25 depicts the system with the controller accurately tracking the optimal

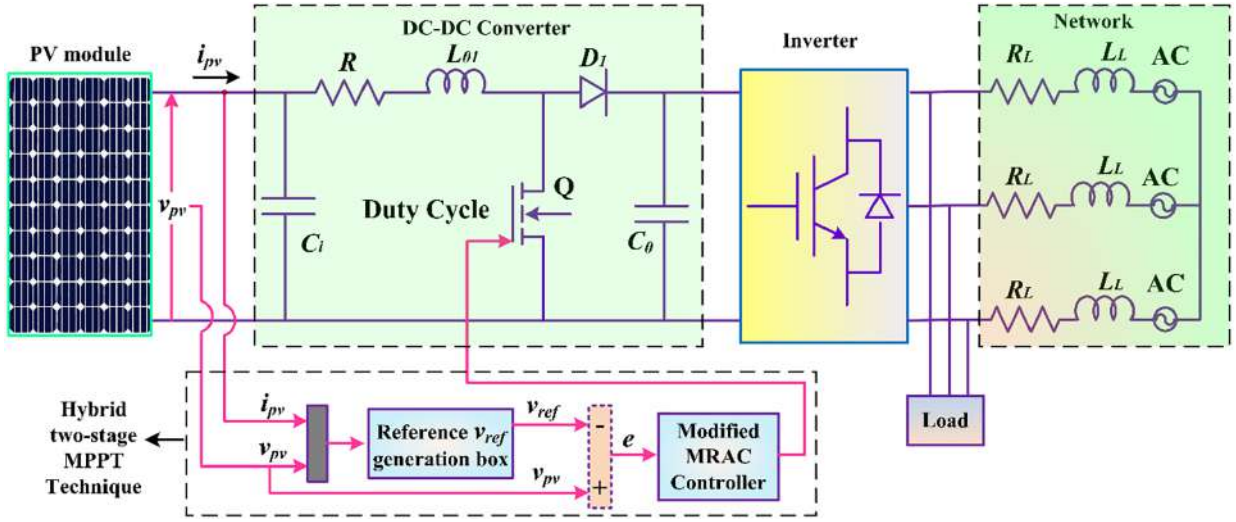

FIGURE 24 Schematic diagram of grid integrated PV.

TABLE 6 Simulation parameters for three phase grid-integrated system.

Parameter	Value	Parameter	Value
Nominal power	50 kW	Per phase filter inductance	2.8 mH
Grid voltage	380 V	PV Panel (17 parallel and 14 series)	213.15 W MPP and 29 V MPP
DC link capacitance	330 μF	Grid frequency	50 Hz
Inductor resistance	0.7 Ω	Sampling time	10 μs
Per phase filter capacitance	5 μF		

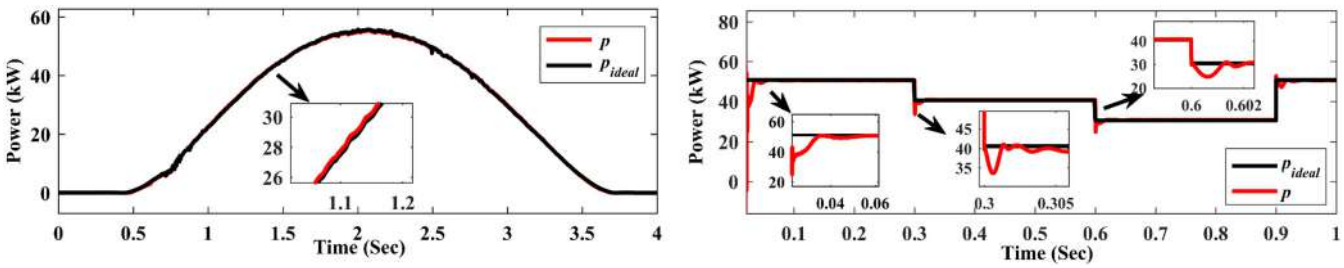

FIGURE 25 The PV and ideal power in grid connected condition.

power with almost zero oscillations. As can be seen in Figure 26, a THD study of grid current has been performed. The obtained THD is 2.92%. The IEEE 519 standard specifies a maximum THD of 5%, which is met by the proposed scheme's THD as shown in Figure 26.

Scenario 2: Irradiation curve with two cloud effect

Figure 27 depicts a simulation comparison between the ideal power and the maximum power that can be obtained from PV systems when the weather is cloudy. Based on Figure 27 and its corresponding zoom view, it's clear that the proposed scheme easily tracks the ideal power under cloudy weather conditions. Figures 28 and 29A,B, illustrate the grid current that demonstrates the proposed MPPT scheme's proper synchronisation and effectiveness. In this case, the THD was found to be 2.71%. The IEEE 519 standard specifies a maximum THD of 5%, which is met by the proposed scheme's THD as shown in Figure 30.

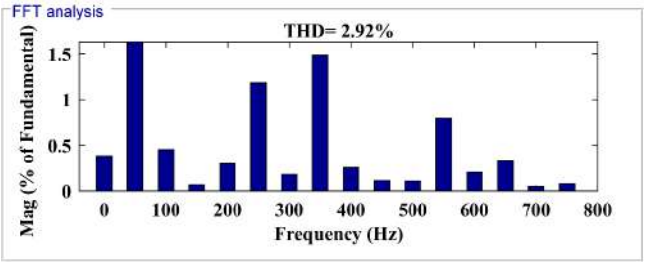

FIGURE 26 THD of grid current.

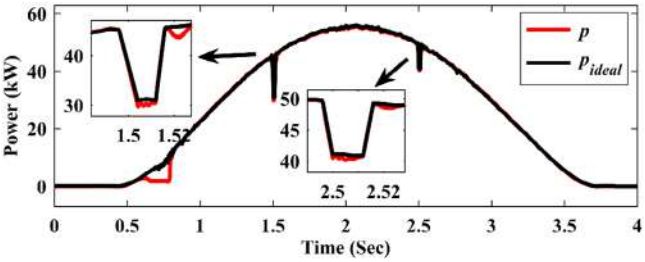

FIGURE 27 The PV and ideal power under cloudy weather.

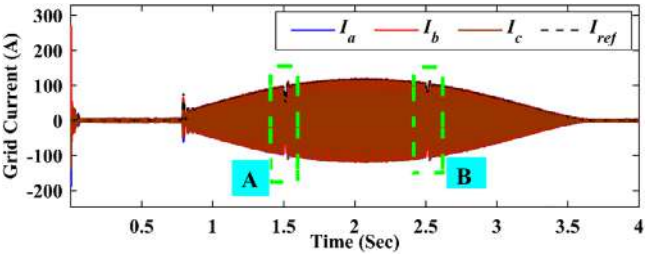

FIGURE 28 Grid current.

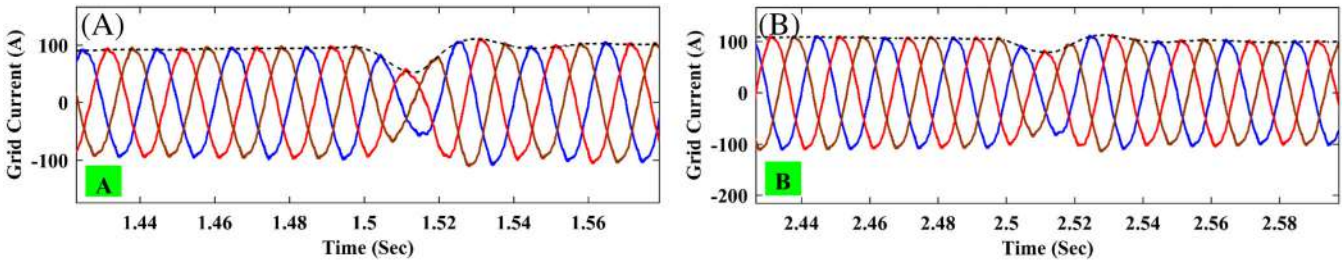

FIGURE 29 Current tracking results in cloudy weather, (A) "A" and (B) "B".

5.4 | Level-IV uncertainty

5.4.1 | Real-time simulator OP4510

Experimental assessment of the recommended MPPT strategy was carried out in the lab using an OPAL-RT (OP4510) simulator as illustrated in Figure 31. It has a built-in system called RT-LAB, which is one of its features. The host computer and RT simulator are the two parts of the system. The OPAL-RT environment is used to build the Simulink model in real

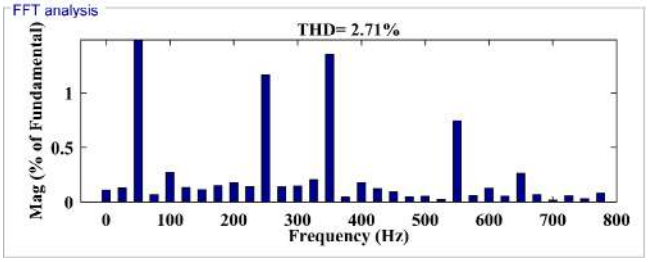

FIGURE 30 THD of grid current.

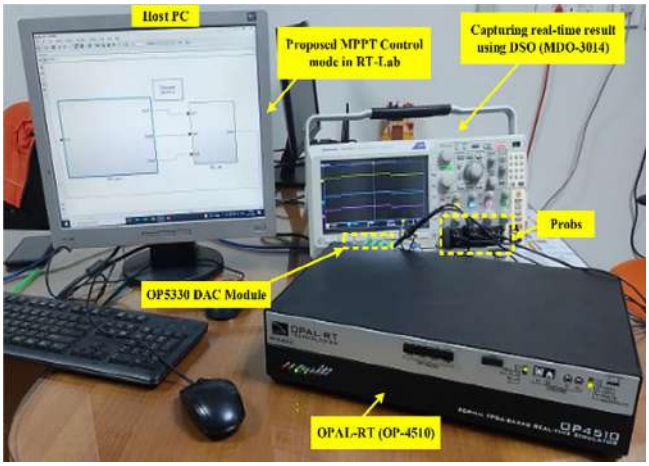

FIGURE 31 Experimental setup.

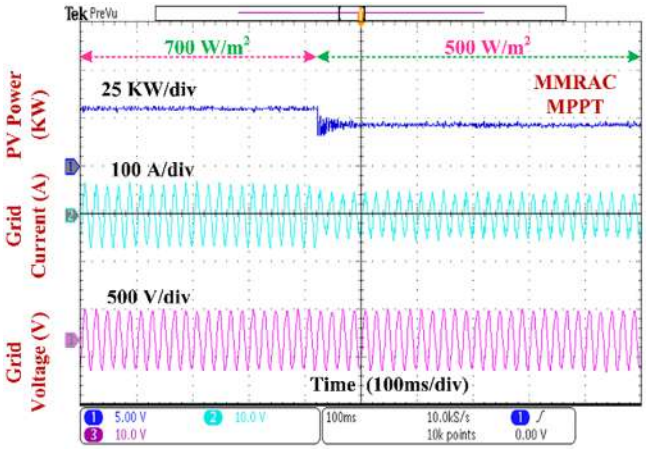

FIGURE 32 PV power, grid current and grid voltage under high to low radiation level.

time and executed using the OPAL-RT simulator. On DSO, the signal including PV power, voltage, current, grid current and grid voltage were observed.

Figures 32 and 33 exhibit the waveforms of PV power, grid current and grid voltage when the solar radiation level changes from high to low and low to high level, respectively. They show the grid current and grid voltage waveforms observes in practical conditions under transient weather circumstances. These waveforms demonstrate the outstanding performance of MMRAC controller, as the grid current is in sinusoidal alignment with grid voltage. The experimental outcomes of PV current, power, and voltage obtained through OPAL-RT platform validate the efficacy of recommended

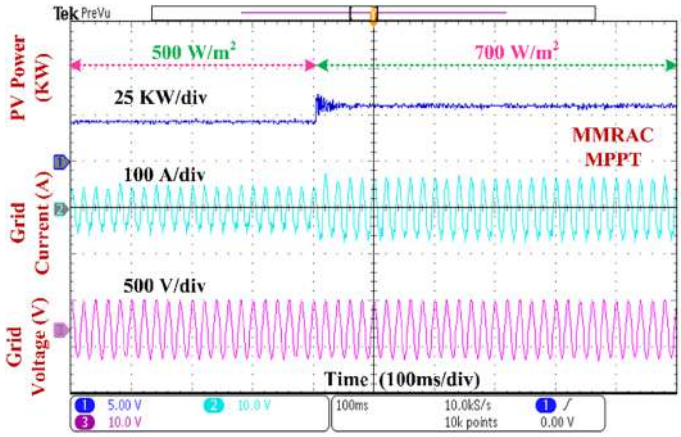

FIGURE 33 PV power, grid current and grid voltage under low to high radiation level.

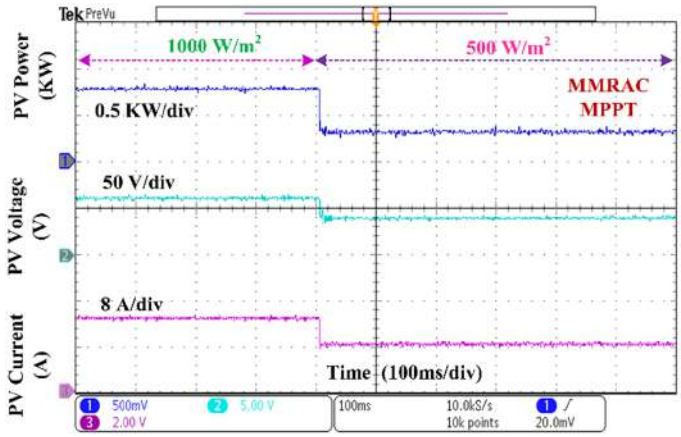

FIGURE 34 PV power, voltage and current tracking ability of the MMRAC scheme.

MPPT controller design, which is demonstrated in Figure 34. It displays the experimental waveform achieved using the proposed MPPT technique, which ensure precise and efficient tracking of PV power even when exposed to fluctuating solar radiation.

The power tracking, PV voltage and current performance of the ANFIS and P&O strategies, in response to variations in solar radiation, is depicted in Figure 35A,B, respectively. Compared to the P&O approach, the ANFIS approach exhibits low oscillations around MPP. The proposed MMRAC scheme demonstrates outstanding power tracking performance compared to P&O, and ANFIS approaches. Additionally, the effectiveness of suggested MPPT strategy is assessed under changing temperature and simultaneously changing solar radiation & temperature profile, as illustrated in Figure 36A,B respectively.

The practical outcomes indicate that, in comparison to P&O and ANFIS, the recommended MPPT strategy achieves optimal PV power tracking while maintaining zero disturbance in the vicinity of the MPP region.

The evaluation of performance is reliant on six main factors, all of which may be simplified by initialising a radar chart. The complexity, capability at PSC, tracking time, efficiency, grid-integration and steady-state oscillations are taken into consideration for evaluating the controller performance. The radar chart diagram of 10 distinct MPPT strategies is shown in Figure 37. The radar plot's contour is normalised from 1 (minimum) to 4 (maximum). The method's strength like very fast, low oscillations, simple algorithm, high efficiency, operated at PSC and three phase grid integration can be seen in the maximum sale, while its weakness like slow, high oscillation, complex algorithm, low efficiency, not operated under PSC and three phase grid connected conditions can be seen on the minimum scale.

This article provides a case study to help readers better grasp how performance is evaluated. In terms of tracking speed, there are four distinct classes: slow (>1 s), medium (0.1–1 s), rapid (0.1–0.01 s), and very fast (0.01–0.001 s). Efficiency

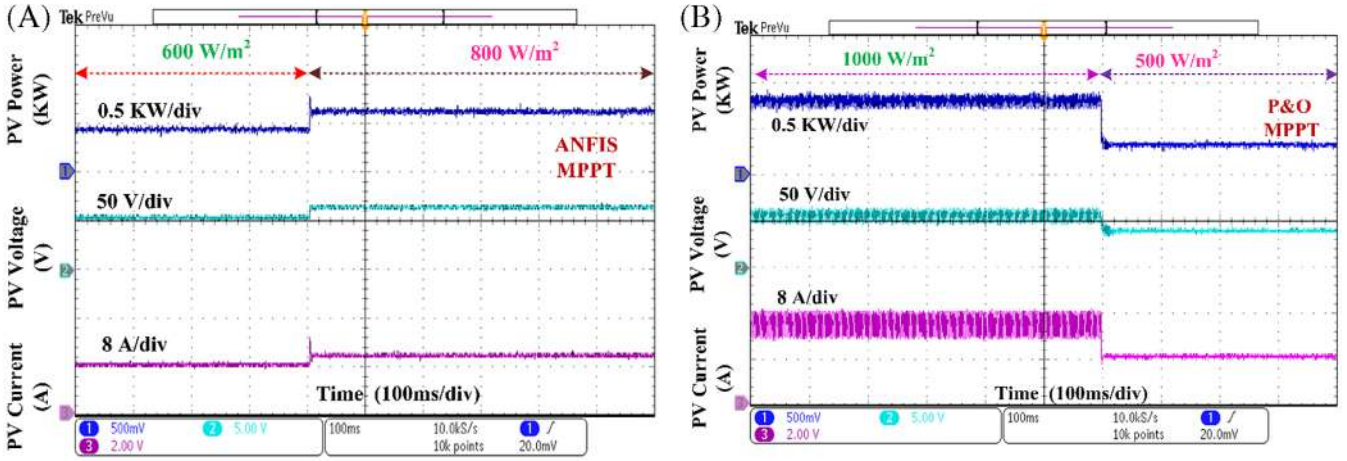

FIGURE 35 PV power, voltage and current tracking ability (A) ANFIS (B) P&O technique.

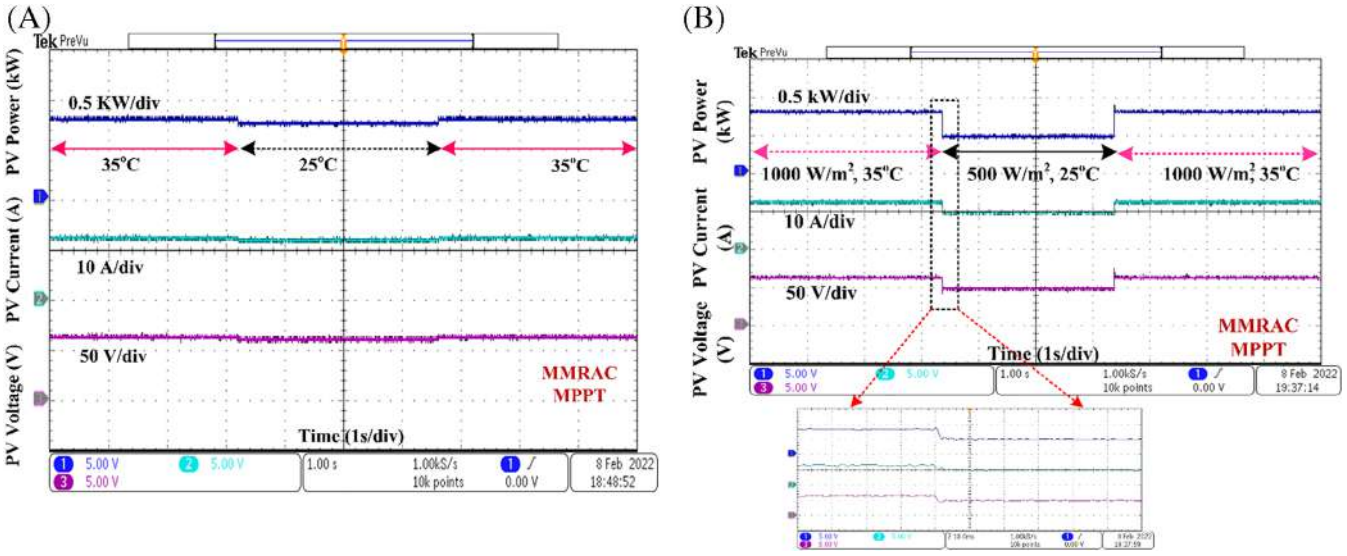

FIGURE 36 PV power, voltage and current tracking ability of the proposed MMRAC scheme (A) temperature (B) both radiation and temperature variation.

levels between (>99.50%), (99%–99.5%), (98%–99%), and (<98%) are categorised as extremely high, high, medium, and low, respectively. The wide contour area performs better than the little contour area on the spider diagram. There is currently sufficient evidence to conclude that the suggested MMRAC-MPPT method is the most superior with respect to accuracy, complexity, speed, efficiency, and environmental effect.

6 | CONCLUSIONS

A novel adaptive strategy called as modified model reference adaptive control (MMRAC) has been developed for MPPT under uniform, partially shaded, and three-phase grid-connected PV system. The MPPT problem transforms into a time-bounded nonlinear problem in rapidly changing atmospheric conditions, hence this technique is the best choice for quickly tracking the MPP. The MMRAC controller was designed to do four goals: (i) decreased oscillation close to MPP (ii) straightforward design and implementation (iii) capacity to adjust under changing weather conditions (iv) fast tracking response. In order to assess MPPT performance of the MMRAC controller, four distinct degrees of uncertainty were used. Additionally, the MMRAC performance was assessed against those of cutting-edge strategies including ANFIS,

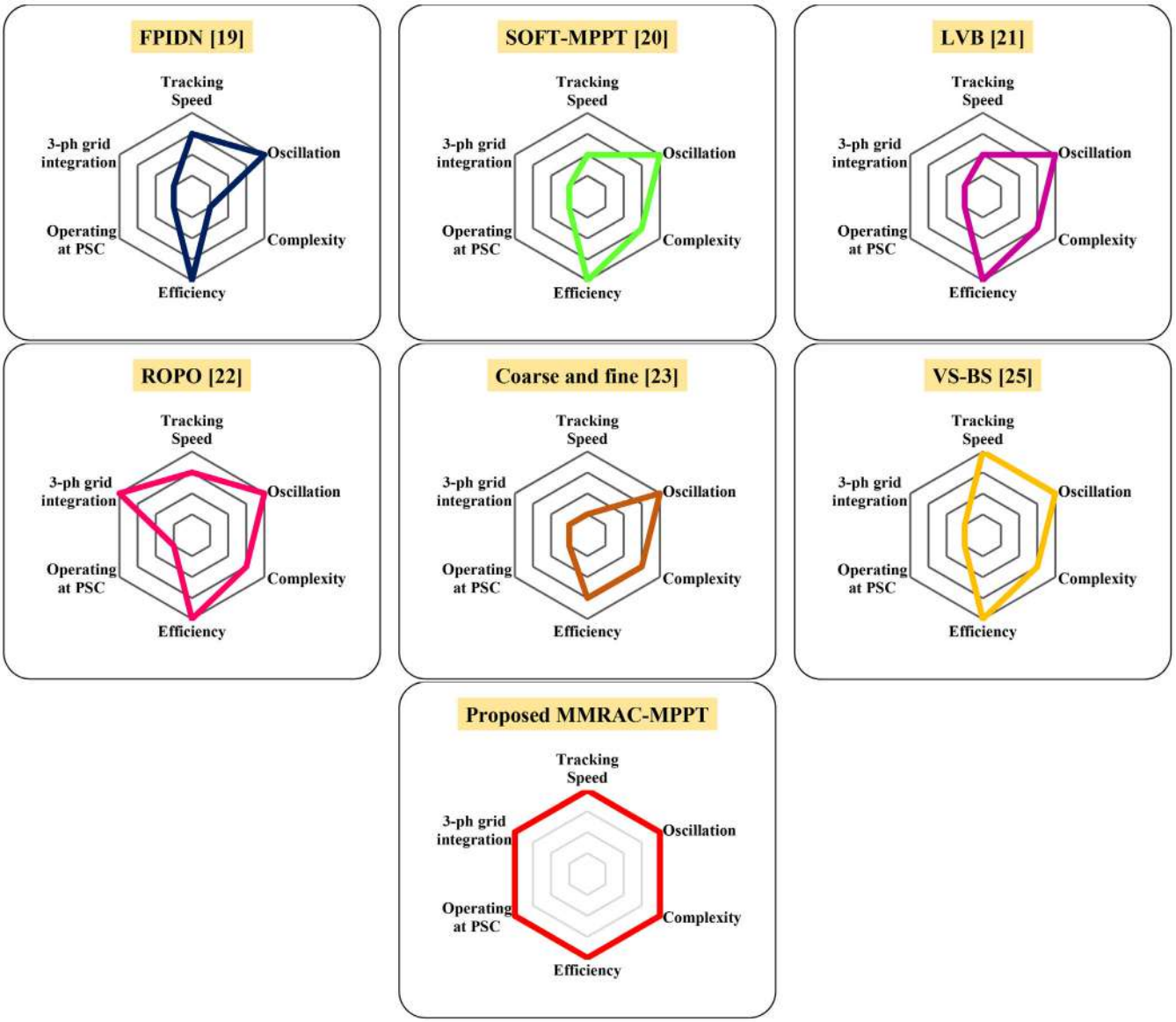

FIGURE 37 Radar graph depicting the relative merits of the various MPPT approaches.

INC, VSPO, and P&O. The MMRAC-MPPT has excellent tracking efficiency between 99.07% and 99.96%, while P&O is in between 96.02% and 97.80%, VSPO is in between 98.05% and 98.70%, INC is in between 97.12% and 97.80% and ANFIS is in between 98.74% and 99.50% for all the considered states. The suggested MPPT has the lowest tracking power loss compared to the other strategies, and negligible oscillations around MPP. This makes the technique the leading in terms of efficiency. The time requirement for the suggested MPPT method is only 3.8 ms to achieve MPP, which is about 52 times faster than P&O and INC, 42 times than VSPO, and six times faster than ANFIS. Compared to other methods, the proposed scheme has the lowest error at MPP. Also, the performance is compared with ANFIS and P&O under four distinct shading pattern conditions. Based on the results, the MMRAC-MPPT strategy harvests maximum power and proves the least power loss due to shading. The recommended controller is able to follow the GMPP under PSC with dynamic irradiance changes. In addition, the MMRAC-MPPT performance is verified using a three-phase grid, and the findings reveal that the grid current's power quality satisfies the IEEE 519 standard. Real-time verification with the OPAL-RT simulator (OP4510) further demonstrates the practicability of the suggested strategy.

CONFLICT OF INTEREST STATEMENT

The authors declare that they have no conflict of interest.

DATA AVAILABILITY STATEMENT

The data that support the findings of this study are available from the corresponding author upon reasonable request.

ORCID

Saibal Manna https://orcid.org/0000-0003-0703-1371

REFERENCES

1. Ali AIM, Mohamed HRA. Improved P&O MPPT algorithm with efficient open-circuit voltage estimation for two-stage grid-integrated PV system under realistic solar radiation. *Int J Electr Power Energy Syst*. 2022;137:107805. doi:10.1016/j.ijepes.2021.107805
2. Singh DK, Akella AK, Manna S. Deterministic and probabilistic analysis of different empirical models to estimate monthly mean diffuse solar radiation for composite climatic region of India. *Environ Prog Sustain Energy*. 2022;41(6):1-22. doi:10.1002/ep.13917
3. Zhang Y, Ren J, Pu Y, Wang P. Solar energy potential assessment: a framework to integrate geographic, technological, and economic indices for a potential analysis. *Renew Energy*. 2020;149:577-586. doi:10.1016/j.renene.2019.12.071
4. Motahhir S, El Hammoumi A, El Ghzizal A. The most used MPPT algorithms: review and the suitable low-cost embedded board for each algorithm. *J Clean Prod*. 2020;246:118983. doi:10.1016/j.jclepro.2019.118983
5. Mao M, Cui L, Zhang Q, Guo K, Zhou L, Huang H. Classification and summarization of solar photovoltaic MPPT techniques: a review based on traditional and intelligent control strategies. *Energy Rep*. 2020;6:1312-1327. doi:10.1016/j.egyr.2020.05.013
6. Wasim MS, Amjad M, Habib S, Abbasi MA, Bhatti AR, Muyeen SM. A critical review and performance comparisons of swarm-based optimization algorithms in maximum power point tracking of photovoltaic systems under partial shading conditions. *Energy Rep*. 2022;8:4871-4898. doi:10.1016/j.egyr.2022.03.175
7. Ali MN, Mahmoud K, Lehtonen M, Darwish MMF. An efficient fuzzy-logic based variable-step incremental conductance MPPT method for grid-connected PV systems. *IEEE Access*. 2021;9:26420-26430. doi:10.1109/access.2021.3058052
8. Singh DK, Akella AK, Manna S. A novel robust maximum power extraction framework for sustainable PV system using incremental conductance based MRAC technique. *Environ Prog Sustain Energy*. 2023;42:e14137. doi:10.1002/ep.14137
9. Manna S, Singh DK, Akella AK. A review of control techniques for wind energy conversion system. *Int J Eng Technol Innov*. 2023;13(1):40-69. doi:10.46604/ijeti.2023.9051
10. Bollipo RB, Mikkili S, Bonthagorla PK. Critical review on PV MPPT techniques: classical, intelligent and optimisation. *IET Renew Power Gener*. 2020;14(9):1433-1452. doi:10.1049/iet-rpg.2019.1163
11. Aminnejhad H, Kazeminia S, Aliasghary M. Robust sliding-mode control for maximum power point tracking of photovoltaic power systems with quantized input signal. *Optik*. 2021;247:167983. doi:10.1016/j.ijleo.2021.167983
12. Tavakoli A, Forouzanfar M. A self-constructing Lyapunov neural network controller to track global maximum power point in PV systems. *Int Trans Electr Energy Syst*. 2020;30(6):1-15. doi:10.1002/2050-7038.12391
13. Bisht R, Sikander A. An improved method based on fuzzy logic with beta parameter for PV MPPT system. *Optik*. 2022;259:168939. doi:10.1016/j.ijleo.2022.168939
14. Harrag A, Messalti S. PSO-based SMC variable step size P&O MPPT controller for PV systems under fast changing atmospheric conditions. *Int J Numer Model: Electron Netw Dev Fields*. 2019;32:e2603. doi:10.1002/jnm.2603
15. Feroz Mirza A, Mansoor M, Ling Q, Khan MI, Aldossary OM. Advanced variable step size incremental conductance MPPT for a standalone PV system utilizing a GA-tuned PID controller. *Energies*. 2020;13(16):4153. doi:10.3390/en13164153
16. Manna S, Akella AK, Singh DK. Implementation of a novel robust model reference adaptive controller-based MPPT for stand-alone and grid-connected photovoltaic system. *Energy Sources A: Recov Utiliz Environ Effects*. 2023;45(1):1321-1345. doi:10.1080/15567036.2023.2178550
17. Verma P, Garg R, Mahajan P. Asymmetrical fuzzy logic control based mppt algorithm for stand-alone pv system under partially shaded conditions. *Sci Iran*. 2019;27(6):3162-3174. doi:10.24200/sci.2019.51737.2338
18. Manna S, Akella AK, Singh DK. Novel Lyapunov-based rapid and ripple-free MPPT using a robust model reference adaptive controller for solar PV system. *Protect Control Modern Power Syst*. 2023;8(13):1-25. doi:10.1186/s41601-023-00288-9
19. Srinivasarao P, Peddakapu K, Mohamed MR, Deepika KK, Sudhakar K. Simulation and experimental design of adaptive-based maximum power point tracking methods for photovoltaic systems. *Comput Electr Eng*. 2021;89:106910. doi:10.1016/j.compeleceng.2020.106910
20. Bhattacharyya S, Kumar PDS, Samanta S, Mishra S. Steady output and fast tracking MPPT (SOFT-MPPT) for P&O and InC algorithms. *IEEE Trans Sustain Energy*. 2021;12(1):293-302. doi:10.1109/tste.2020.2991768
21. Kumar V, Ghosh S, Naidu NKS, Kamal S, Saket RK, Nagar SK. Load voltage-based MPPT technique for standalone PV systems using adaptive step. *Int J Electr Power Energy Syst*. 2021;128:106732. doi:10.1016/j.ijepes.2020.106732
22. Pathak PK, Yadav AK, Alvi PA. Reduced oscillations based perturb and observe solar maximum power point tracking scheme to enhance efficacy and speed of a photovoltaic system. *J Eng Res*. 2022:1-13. doi:10.36909/jer.13569
23. Kavya M, Jayalalitha S. A novel coarse and fine control algorithm to improve maximum power point tracking (MPPT) efficiency in photovoltaic system. *ISA Trans*. 2022;121:180-190. doi:10.1016/j.isatra.2021.03.036
24. Kumar V, Mitra A, Shaklya O, Sharma S, Rana KPS. An adaptive robust fuzzy PI controller for maximum power point tracking of photovoltaic system. *Optik*. 2022;259:168942. doi:10.1016/j.ijleo.2022.168942
25. Charaabi A, Zaidi A, Barambones O, Zanzouri N. Implementation of adjustable variable step based backstepping control for the PV power plant. *Int J Electr Power Energy Syst*. 2022;136:107682. doi:10.1016/j.ijepes.2021.107682

26. Priyadarshi N, Padmanaban S, Holm-Nielsen JB, Blaabjerg F, Bhaskar MS. An experimental estimation of hybrid ANFIS–PSO-based MPPT for PV grid integration under fluctuating sun irradiance. *IEEE Syst J*. 2020;14(1):1218-1229. doi:10.1109/jsyst.2019.2949083
27. Priyadarshi N, Padmanaban S, Kiran Maroti P, Sharma A. An extensive practical investigation of FPSO-based MPPT for grid integrated PV system under variable operating conditions with anti-islanding protection. *IEEE Syst J*. 2019;13(2):1861-1871. doi:10.1109/jsyst.2018.2817584
28. Priyadarshi N, Sanjeevikumar P, Bhaskar M, Azam F, Taha IBM, Hussien MG. An adaptive TS-fuzzy model based RBF neural network learning for grid integrated photovoltaic applications. *IET Renew Power Gener*. 2022;16(14):3149-3160. doi:10.1049/rpg2.12505
29. Priyadarshi N, Bhaskar MS, Sanjeevikumar P, Azam F, Khan B. High-power DC-DC converter with proposed HSFNA MPPT for photovoltaic based ultra-fast charging system of electric vehicles. *IET Renew Power Gener*. 2022:1-13. doi:10.1049/rpg2.12513
30. Priyadarshi N, Bhaskar MS, Modak P, Kumar N. A novel optimized orthogonal hybrid firefly based ant colony method occupying MPPT for single stage PV water pumping applications. Paper presented at: 2022 IEEE 2nd International Conference on Sustainable Energy and Future Electric Transportation (SeFeT); 2022. doi:10.1109/sefet55524.2022.9909016
31. Priyadarshi N, Maroti PK, Hussien MG. Extensive performance investigation of Luo converter-based modified firefly maximum point tracking algorithm for permanent magnet synchronous motor-driven photovoltaic pumping system. *IET Renew Power Gener*. 2022:1-11. doi:10.1049/rpg2.12520
32. Priyadarshi N, Padmanaban S, Bhaskar MS, Khan B. An experimental performance verification of continuous mixed P-norm based adaptive asymmetrical fuzzy logic controller for single stage photovoltaic grid integration. *IET Renew Power Gener*. 2022:1-11. doi:10.1049/rpg2.12410
33. Manna S, Singh DK, Akella AK, et al. Design and implementation of a new adaptive MPPT controller for solar PV systems. *Energy Rep*. 2023;9:1818-1829. doi:10.1016/j.egyr.2022.12.152
34. Khanna R, Zhang Q, Stanchina WE, Reed GF, Mao Z-H. Maximum power point tracking using model reference adaptive control. *IEEE Trans Power Electron*. 2014;29(3):1490-1499. doi:10.1109/tpel.2013.2263154
35. Manna S, Akella AK, Singh DK. A novel MRAC-MPPT scheme to enhance speed and accuracy in PV systems. *Iran J Sci Technol Trans Electr Eng*. 2022;47(1):233-254. doi:10.1007/s40998-022-00542-0
36. Chen M, Ma S, Wu J, Huang L. Analysis of MPPT failure and development of an augmented nonlinear controller for MPPT of photovoltaic systems under partial shading conditions. *Appl Sci*. 2017;7(1):95. doi:10.3390/app7010095

How to cite this article: Manna S, Singh DK, Akella AK. Hybrid two-stage adaptive maximum power point tracking for stand-alone, grid integration, and partial shaded PV system. *Int J Adapt Control Signal Process*. 2023;1-31. doi: 10.1002/acs.3684